Measurement report: Formation and brownness of aqueous secondary organic aerosol from the aged biomass-burning emissions in the Sichuan Basin, China

Chao Peng[1,2,3,4], Yan Ding[4], Zhenliang Li[1,2,3], Tianyu Zhai[4], Xinping Yang[4], Mi Tian[6], Yang Chen[5], Xin Long[5], Haohui Tang[6], Guangming Shi[7], Liuyi Zhang[8], Kangyin Zhang[8], Fumo Yang[7], and Chongzhi Zhai[1,2,3]

[1]Chongqing Academy of Ecology and Environmental Sciences, Chongqing, 401336, China

[2]Chongqing Branch Academy of Chinese Research Academy of Environmental Sciences, Chongqing, 401336, China

[3]Chongqing Key Laboratory of Urban Atmospheric Environment Observation and Pollution Prevention, Chongqing, 401336, China

[4]Chinese Research Academy of Environmental Sciences, Beijing 100012, China

[5]Chongqing Institute of Green and Intelligent Technology, Chinese Academy of Sciences, Chongqing, 400714, China

[6]College of Environment and Ecology, Chongqing University, Chongqing, 400045, China

[7]College of Carbon Neutrality Future Technology, Sichuan University, Chengdu, 610065, China

[8]Chongqing Three Gorges University, Wanzhou, 404000, China

Correspondence: Chao Peng (pengchao0623@sina.com) and Chongzhi Zhai (czz66818@sina.com)

Abstract. Secondary organic aerosol (SOA), formed via complex chemical mechanisms, is a major contributor to atmospheric aerosol pollution and climate forcing worldwide. Aqueous-phase oxidation serves as an important pathway for SOA formation, with aqueous SOA (aqSOA) exhibiting light absorption across the ultraviolet–visible range. This study investigates the formation and absorption properties of aqSOA in the Sichuan Basin, China. Results indicate that aqSOA mainly originated from aged biomass-burning emissions through aqueous-phase processing rather than from gas-phase photochemical oxidation, particularly under high aerosol liquid water content conditions during pollution periods. Substantial enhancement of brown carbon absorption by SOA was observed between 370 and 660 nm (27.5%−43.2%). These findings highlight the significant contribution of aqSOA formation from aged biomass-burning emissions to the brown carbon budget and absorption, especially at night. The mean aerosol absorption Ångström exponents between 370 and 880 nm ($AAE_{370–880}$) were 1.95, which is higher than the values reported for fresh and photochemically aged biomass-burning emissions. This study elucidates the formation and light-absorbing characteristics of aqSOA derived from aged biomass-burning emissions and highlights the important role of aqueous-phase reactions in aerosol pollution and radiative absorption.

Keywords: Particulate matter; Secondary organic aerosol; Aqueous-phase oxidation; Aged biomass-burning emissions; Brown carbon

1 Introduction

Organic aerosol (OA) constitutes a dominant fraction (20−90%) of atmospheric aerosol, with significant implications for air quality and climate forcing (Jimenez et al., 2009). Field observations consistently indicate that secondary OA (SOA), formed by the atmospheric oxidation of volatile organic compounds (VOCs) and primary OA (POA), accounts for most OA worldwide (Ervens et al., 2011; Huang et al., 2014; Kourtchev et al., 2016). Recent results demonstrate that aqueous-phase oxidation serves as an important pathway for SOA formation, and aqueous SOA (aqSOA) exhibits light absorption across the ultraviolet–visible (UV–Vis) range (Gilardoni et al., 2016; Lim et al., 2010; McNeill 2015; Powelson et al., 2014; Sun et al., 2010). However, the formation mechanisms and absorption properties of aqSOA remain poorly understood, which hinders efforts to improve air quality and reduce uncertainties in global climate estimates.

Several studies suggest that aqSOA represents a major component of SOA formed in fog, clouds and aerosol water (Ervens et al., 2011; Ortiz-Montalvo et al., 2012; Tan et al., 2012; Xu et al., 2022). Oxygenated VOCs with high water solubility and low Henry's law constants, such as methylglyoxal and glycolaldehyde, are important aqSOA precursors (Ortiz-Montalvo et al., 2012; Tan et al., 2012). Limited laboratory studies have demonstrated that levoglucosan and phenolic species produced from biomass burning can also act as aqSOA precursors (Yu et al., 2016; Zhao et al., 2014). Gilardoni et al. (2016) reported direct ambient observations of aqSOA formation from biomass-burning emissions in fog, water and wet aerosol. Additionally, recent studies have reported that aqSOA with high molecular weight (e.g., 4-ethylphenol), formed through aqueous-phase photochemical oxidation, can exhibit strong light absorptivity in the UV range (Herrmann et al., 2015; Ye et al., 2019). Furthermore, previous laboratory studies have demonstrated that certain aqSOA components, such as π-conjugated compounds and imidazoles with C=N bonds, produced by aldol condensation and aqueous-phase carbonyl compound reactions, respectively, strongly absorb light in the near-UV region (Drozd and

McNeill, 2014; Kampf et al., 2012; Nozière and Esteve, 2007; Powelson et al., 2014). Despite numerous studies on the formation and optical properties of aqSOA, limited ambient observations still hinder a better understanding of its role in atmospheric chemistry and climate.

China has experienced severe $PM_{2.5}$ pollution under stagnant high-humidity conditions, during which SOA, a major $PM_{2.5}$ component, originated largely from fossil fuel combustion and biomass burning (Huang et al., 2014; Wang et al., 2016; Wang et al., 2021; Xu et al., 2022). Field observations indicate that highly oxidized SOA can form through aqueous-phase processing driven by acid-catalyzed oxidation (Meng et al., 2020; Xu et al., 2017), and aqSOA is derived from biomass-burning OA (BBOA) and fossil-fuel OA through aqueous-phase reactions (Wang et al., 2021; Zhao et al., 2019). Limited laboratory studies have reported that aqueous-phase reactions serve as an important oxidation pathway for nitrophenol products such as 5-nitrovanillin and 4-nitroguaiacol, which exhibit strong UV absorption and higher formation and transformation rates in more acidic solutions (Kroflic et al., 2015; Li et al., 2023; Pang et al., 2019; Yang et al., 2021). However, observations of aqSOA formation and optical properties in China remain limited, with most research focusing on the North China Plain (NCP). Similar to the NCP, the Sichuan Basin (SCB), characterized by high humidity and frequent biomass burning, is also the main region with severe aerosol pollution in China (Tian et al., 2019; Wang et al., 2018; Yang et al., 2011).

Previous research has reported that aqSOA from different regions can exhibit distinct formation mechanisms and optical properties due to varying emission sources and ambient conditions (Bao et al., 2023; Bao et al., 2024; Wang et al., 2021; Xu et al., 2017). Wang et al. (2021) reported the rapid aqueous-phase conversion of fossil-fuel primary OA (FF-POA) to aqSOA under high-humidity conditions during a winter haze event in Beijing, China, with the resulting aqSOA exhibiting substantially lower light absorption than its primary precursor due to decreased aromaticity. Similarly, Huang et al. (2023) demonstrated that the aqueous-phase oxidation of fossil fuel combustion emissions played a critical role in SOA formation under high relative

humidity (RH) conditions during winter. Xu et al. (2022) reported that biomass burning is a significant non-fossil source of aqSOA under high RH and high aerosol liquid water content (ALWC), especially during the fall-to-winter period, when open burning of post-harvest agricultural crop residues is widespread in China. While aqSOA formation has been extensively studied during winter, autumn—despite featuring both high ALWC and strong biomass-burning emissions—has received considerably less attention (Feng et al., 2022; Qiu et al., 2016; Zhao et al., 2019). In contrast to these studies in the NCP, research in the SCB has reported that the effect of aqueous-phase reactions on oxygenated OA (OOA) formation was significant when ALWC was below 200 μg m^{-3}, but became insignificant when ALWC exceeded 200 μg m^{-3}. Additionally, aqueous-phase oxidation probably did not contribute to the decay of brown carbon (BrC) during summer in the SCB (Bao et al., 2024). In the SCB, autumn is the typical biomass-burning season following the harvest of rape and rice, during which biomass burning contributes significantly more to OA than in other seasons (Chen et al., 2017; Tao et al., 2014; Yang et al., 2019). In summary, the intensive biomass-burning emissions and high ALWC during autumn in the SCB likely result in aqSOA formation pathways that differ from those in other seasons. To date, limited studies have explored the dynamic evolution and optical properties of aqSOA in the SCB, especially during autumn, leaving ambient aqSOA processing poorly understood. Therefore, a more detailed characterization of the aqSOA formation and optical properties is important to reveal the key factors contributing to haze formation in this region.

In this study, a time-of-flight aerosol chemical speciation monitor (ToF-ACSM) and a series of collocated instruments were deployed to characterize the dynamic evolution of aqSOA from biomass burning under real ambient conditions. The study was conducted in a typical city with relatively severe air pollution in the SCB from October 21 to November 23, 2022. Observations revealed that haze formation was significantly driven by BBOA and aqSOA. This study demonstrates that aqSOA forms from aged BBOA through aqueous-phase reactions. Furthermore, the results demonstrate that aqSOA derived from aged BBOA exhibits strong UV absorption and

contributes to positive radiative forcing. These results elucidate the formation and light-absorbing properties of aqSOA from aged biomass-burning emissions, providing insights for improved simulations of its atmospheric and climatic impacts.

2 Methods

2.1 Sampling site

An intensive field campaign investigating the chemical and physical properties of aerosols was conducted at a site in Yongchuan, China, (29°21′25″ N, 105°54′6″ E), a city experiencing severe aerosol pollution, from October 21 to November 23, 2022. This site is representative of an urban environment, surrounded by restaurants, shopping malls, and residential buildings, and is located in a parallel ridge-and-valley area between the two megacities of the SCB (Chongqing center and Chengdu) (Fig. S1). It is primarily influenced by multiple local emission sources, including traffic (arterial roads 600 m to the east and 300 m to the west) and a variety of residential activities such as biomass burning and fossil fuel combustion. The absence of dynamic interference from neighbouring buildings allowed the measurements to clearly capture the characteristics and evolution of haze pollution at this site.

2.2 Instrumentation

During the campaign, non-refractory aerosol (NR-$PM_{2.5}$) species, including OA, ammonium (NH_4), nitrates (NO_3), sulfates (SO_4), and chlorides (Chl), were measured online using the ToF-ACSM (Aerodyne Research Inc.). Ambient aerosols were pumped into the ToF-ACSM at a flow rate of 3 L min^{-1} through a $PM_{2.5}$ cyclone (URG-2000-30ED) and a Nafion dryer (MD-110-48S, Perma Pure, Inc.), reducing the RH to below 30%. The measurement principle has been described in detail in previous studies (Fröhlich et al., 2013; Ng et al., 2011c).

Aerosol light absorption (Abs_λ) and equivalent black carbon (BC_λ) mass concentrations were measured in real time at seven wavelengths (370, 470, 520, 590, 660, 880, and 950 nm) using an aethalometer (AE33, Magee Scientific). Sampled

particles were dried using a Nafion dryer (MD-70024S-3, Perma Pure, Inc.) before measurements. The light attenuation coefficients were converted to Abs_{λ} using the real-time compensation parameter, and the nonlinear loading effects of quartz filters were corrected online through parallel measurements of attenuation values (ATN1 and ATN2) (Coen et al., 2010; Drinovec et al., 2015). The scattering effects of quartz filters were modified automatically by a fixed multiple-scattering parameter (2.14) (SI Text S3). Detailed measurement methods and principles of AE33 are described in Drinovec et al. (2015).

During the campaign, gaseous species (including O_3, NO_2, and CO) were continuously measured by gas analyzers (49i, 42i, and 48i, Thermo Scientific) that were maintained and calibrated weekly. Hourly meteorological parameter data, including temperature (T), RH, and $PM_{2.5}$ mass concentrations, were obtained from the National Environmental Monitoring Station, located near our sampling site (http://www.cnemc.cn/, last access: 30 November 2022).

2.3 Data analysis

2.3.1 ToF-ACSM data analysis

The raw mass spectra data measured by the ToF-ACSM were analyzed using Tofware v2.5.13 (Tofwerk AG) in Igor Pro 6.37 (WaveMetrics, Inc.). The ionization efficiency and relative ionization efficiency (RIE) were regularly calibrated using a scanning mobility particle sizer, consisting of a differential mobility analyzer (SMPS 3081A, TSI) and a condensation particle counter (CPC 3775, TSI). A comprehensive overview of the operation and calibration procedures of the ToF-ACSM is provided in Bao et al. (2023). In accordance with previous studies, the default RIE values for OA, NO_3, and Chl were set to 1.4, 1.1, and 1.3, respectively (Canagaratna et al., 2007; Elser et al., 2016). The ionization efficiency value (236 ions pg^{-1}) and RIE values of SO_4 (1.2) and NH_4 (4.3) were estimated from the calibrations of pure ammonium sulfate and ammonium nitrate (ANMF), respectively. Meanwhile, a particle collection efficiency (CE) was introduced to compensate for the particle losses associated with

the particle bounce at the vaporizer, which is affected by aerosol acidity, the contribution of ammonium nitrate, and phase state (Matthew et al., 2008). Middlebrook et al. (2012) developed a CE algorithm for the ToF-ACSM to quantify aerosol species. Their results indicated that a constant CE value of 0.45 should be used when: (1) ANMF is below 40% or (2) particles are either partially or fully neutralized. In this study, aerosol particles were dried using a Nafion dryer (RH < 30%) before sampling by the ToF-ACSM, and ANMF was consistently maintained below 40%. As shown in Fig. S2, the average ratio of the measured NH_4 to the predicted NH_4, which is required to fully neutralize SO_4, NO_3, and Chl, was approximately 1. Under these conditions, the CE value typically used at this site was not affected. The typical default CE value (0.5) was applied throughout the sampling period, which was consistent with previous research (Bao et al., 2025; Peng et al., 2025; Sun et al., 2016a; Sun et al., 2016b; Zhao et al., 2019). While the typical default CE is 10% higher than 0.45, the difference is small, considering the 30% uncertainty determined for CE (Bahreini et al., 2009). Additionally, the strong correlation between NR-$PM_{2.5}$ and $PM_{2.5}$ mass concentrations supports the validity of the CE value (Fig. S3).

The mass spectral matrix of OA for m/z 10−120 was analysed through positive matrix factorization (PMF) with the multilinear engine (ME-2) implemented in SoFi (Source Finder, version 6.3) (Canonaco et al., 2013; Paatero 1999; Paatero and Tapper 1994). Briefly, an unconstrained PMF analysis was performed to determine the number and types of source factors. Subsequently, the constrained ME-2 approach was applied to minimize rotational ambiguity by testing *a*-values from 0 to 1 in steps of 0.1 (Elser et al., 2016; Wang et al., 2019b; Zhong et al., 2021). Ions with a signal-to-noise ratio (SNR) below 0.2 were discarded, whereas those with an SNR between 0.2 and 2 were downweighted by a factor of 2 (Bao et al., 2023; Paatero and Hopke 2003). Finally, five OA factors were resolved with the rotational parameter set to zero (f_{peak} = 0), including three POA factors (BBOA, coal-combustion OA (CCOA), and hydrocarbon-like OA (HOA)) and two SOA factors (OOA and aqSOA) (Fig. S9 and S10). Detailed diagnostic plots of the PMF results are presented in the Supporting

Information (Fig. S4−S10), and the details of OA source apportionment procedures are described in SI Text S1.

2.3.2 Aerosol liquid water content

ALWC is controlled by meteorological conditions (T and RH) as well as by inorganic and OA components. During the campaign, ALWC controlled by the inorganic fraction was estimated with the ISORROPIA-II thermodynamic model, based on mass concentrations of ammonium, nitrate, sulfate, and chloride measured by the ToF-ACSM, together with the meteorological parameters (T and RH) from the National Environmental Monitoring Station (Fountoukis and Nenes, 2007). The calculations were performed in forward type and metastable mode within ISORROPIA-II (Hennigan et al., 2015). The model simulated the thermodynamic equilibrium of the NH_4^+−SO_4^{2-}−NO_3^-−Cl^-−H_2O system and subsequently calculated the ALWC. Following established methods, the organic contribution to ALWC was estimated using the Zdanovskii−Stokes−Robinson mixing rule, as discussed in SI Text S2 (Guo et al., 2015; Huang et al., 2020; Nguyen et al., 2016; Xu et al., 2022). In this study, the ALWC with organic species ranged from 0.1 to 35.2 μg m^{-3}, with an average of 1.9 ± 3.0 μg m^{-3}, accounting for 3.7 ± 2.2% of total ALWC. As organic species had minor effects on total ALWC (< 5%), the ALWC was determined only considering inorganic species (Chen et al., 2021; Guo et al., 2015; Liu et al., 2017).

2.3.3 Light absorption measurements

The Abs_λ was partitioned into contributions from BC and BrC, a group of colored OA compounds, denoted as $Abs_{\lambda,BC}$ and $Abs_{\lambda,BrC}$, respectively, such that $Abs_\lambda = Abs_{\lambda,BC} + Abs_{\lambda,BrC}$, and characterized by the absorption Ångström exponent (AAE) (Laskin et al., 2015). Here, Abs_λ was derived from BC_λ mass concentrations at each wavelength using the mass absorption cross-section (MAC_λ) ($Abs_\lambda = BC_\lambda \times MAC_\lambda$), with MAC_λ values assumed to be 18.47, 14.54, 13.14, 11.58, 10.35, 7.77, and 7.19 m^2 g^{-1} at 370, 470, 520, 590, 660, 880, and 950 nm, respectively

(Drinovec et al., 2015; Zhu et al., 2017). Absorbance at 880 nm (Abs_{880}) was attributed solely to BC. The following formula was used to determine $Abs_{\lambda,BC}$ values (Drinovec et al., 2015; Kirchstetter and Novakov, 2004; Moosmüller et al., 2009; Qin et al., 2018; Wang et al., 2021; Zhu et al., 2017):

$$Abs_{\lambda,BC} = Abs_{880} \times (880/\lambda)^{-AAE_{BC}} \quad (1)$$

$$AAE_{BC} = -\log_{10}(Abs_{880}/Abs_{950}) \div \log_{10}(880/950) \quad (2)$$

A detailed description of $Abs_{\lambda,BC}$ and $Abs_{\lambda,BrC}$ calculations is provided in SI Text S3. Previous studies have demonstrated that AAE_{BC} is sensitive to the refractive index, size distribution, and coating state of carbonaceous aerosols (Gyawali et al., 2009; Lack and Langridge, 2013; Li et al., 2019). In this study, the uncertainties in Abs_{BC} and Abs_{BrC} estimations were analyzed (Text S3). The relative uncertainties of Abs_{BC} and Abs_{BrC} were [−46%, +21%] and [−112%, +42%] at 370 nm, respectively. $Abs_{\lambda,BrC}$ comprises contributions from primary and secondary BrC ($Abs_{\lambda,BrC,pri}$ and $Abs_{\lambda,BrC,sec}$). $Abs_{\lambda,BrC,sec}$ was calculated using the minimum R-squared method (MRS) at each wavelength (Wang et al., 2019b; Wu and Yu, 2016; Wu et al., 2024). Further details on the MRS method and $Abs_{\lambda,BrC,sec}$ estimation are provided in SI Text S3.

The light absorption contribution of each OA component at each wavelength, as analyzed using multiple linear regression (Qin et al., 2018; Xie et al., 2019), is expressed as follows:

$$Abs_{BrC} = a \times [OOA] + b \times [BBOA] + c \times [CCOA] + d \times [aqSOA] + e \times [HOA] \quad (3).$$

where [OOA], [BBOA], [CCOA], [aqSOA], and [HOA] denote the mass concentrations of the corresponding OA components. Coefficients a–e are constants used to optimize the Abs_{λ} of each OA component and are equivalent to MAC values at each wavelength (i.e., a–e at 370 nm represented $MAC_{370,OOA}$, $MAC_{370,BBOA}$, $MAC_{370,CCOA}$, $MAC_{370,aqSOA}$, and $MAC_{370,HOA}$, respectively). Here, the normalized mean bias, root mean square error, and index of agreement were used to evaluate the performance of the multiple linear regression method (SI Text S4) (Li et al., 2011). The index of agreement values for $Abs_{370,BrC}$ and $Abs_{470,BrC}$ were 0.99 and 1.00, respectively, both exceeding 0.95. The slopes of the linear regression between the

AE33-measured and MLR-estimated absorption coefficients were 0.81 and 0.96 for $Abs_{370,BrC}$ and $Abs_{470,BrC}$ (close to unity), respectively. These results indicate good agreement between the AE33 measurement and the MLR-reconstructed $Abs_{370,BrC}$.

3 Results and discussion

3.1 Enhanced OA formation from BBOA and aqSOA during pollution periods

The temporal variations of $PM_{2.5}$ species concentrations, meteorological parameters, $Abs_{370,BrC}$ and $MAC_{370,BrC}$ during the campaign are shown in Fig. 1. Wind speeds were consistently low (0.3 ± 0.2 m s^{-1}), indicating stagnant atmospheric conditions throughout the study period. The average concentrations of O_3 and NO_2 during the campaign were 24.8 ± 16.1 ppb and 14.2 ± 6.8 ppb, respectively. The total $PM_{2.5}$ (BC + NR-$PM_{2.5}$) mass concentrations ranged from 7.0 to 175.5 μg m^{-3}, with an average of 48.4 ± 27.8 μg m^{-3}. The average concentrations of OA, NO_3, SO_4, NH_4, Chl, and BC were 24.1 ± 18.1, 8.3 ± 6.2, 6.2 ± 3.4, 5.2 ± 2.7, 0.2 ± 0.1, and 4.7 ± 2.9 μg m^{-3}, accounting for 46.6 ± 10.7%, 17.7 ± 8.0%, 13.2 ± 4.4%, 11.2 ± 2.7%, 0.3 ± 0.2%, and 10.1 ± 5.5% of total $PM_{2.5}$, respectively. OA accounted for the largest fraction of $PM_{2.5}$, highlighting its significant contribution to $PM_{2.5}$ pollution in the SCB (Bao et al., 2023; Wang et al., 2018). The OA fractions of $PM_{2.5}$ in this study are comparable to those reported in wintertime studies in the SCB and are significantly higher than those observed in winter in other Chinese regions (Table S1). Meanwhile, elevated levels of $Abs_{370,BrC}$ and $MAC_{370,BrC}$, ranging from 5.8 to 210.2 Mm^{-1} (42.4 ± 28.5 Mm^{-1}) and from 0.6 to 7.0 m^2 g^{-1} (2.1 ± 0.9 m^2 g^{-1}), respectively, were observed during the campaign.

According to the Chinese National Ambient Air Quality Standard (GB 3095-2012) (MEP, 2012), the Grade I and Grade II 24-hour limits for $PM_{2.5}$ are 35 μg m^{-3} and 75 μg m^{-3}, respectively. The Grade II limit, based on the WHO Phase-1 interim target (IT-1), is higher than the WHO Air Quality Guideline value (15 μg m^{-3}), the EU daily limit (25 μg m^{-3}), and the U.S. 24-hour standard (35 μg m^{-3}). During the campaign, the mean $PM_{2.5}$ concentration was 1.4 times the Grade I limit (35 μg m^{-3}).

Pollution periods (PP) were defined as days with daily $PM_{2.5}$ mass concentrations exceeding the Grade II limit (75 μg m^{-3}), whereas days with $PM_{2.5}$ below 75 μg m^{-3} were defined as clean periods (CP). During PP, the average mass concentrations of BC + NR-$PM_{2.5}$ and OA were 2.5 and 3.1 times those during CP, respectively, corresponding to 102.3 ± 26.9 and 57.4 ± 22.5 μg m^{-3}. As shown in Fig. 2, the chemical composition of $PM_{2.5}$ differed substantially between PP and CP. Compared with other species, a significantly higher contribution of OA was observed during PP (56.6%) than during CP (46.6%) (Student's t-test, $p < 0.001$) (Fig. 2).

In this study, five OA factors were resolved using the PMF model. More details are provided in SI Text S1, and the mass spectra of these factors are shown in Fig. S9. HOA was characterized by alkyl fragment ion series at $C_nH^+_{2n-1}$ and $C_nH^+_{2n+1}$ (m/z 41, 43, 55, and 57), which are typical of primary combustion emissions (Elser et al., 2016; Lanz et al., 2007). BBOA was identified by prominent signals at m/z 60 (mainly $C_2H_4O_2^+$) and m/z 73 (mainly $C_3H_5O_2^+$), which correspond to fragments of levoglucosan and mannosan from incomplete biomass burning (Alfarra et al., 2007). CCOA showed high signals of unsaturated hydrocarbon ion fragments such as PAH-related ion fragments (m/z 77, 91, 115), indicative of traditional coal combustion (Sun et al., 2016a). OOA was distinguished by a dominant signal at m/z 44 (mainly CO_2^+) and a strong correlation with oxygenated ions (Ng et al., 2011b). AqSOA also correlated strongly with oxygenated ions, such as m/z 43 (mainly $C_2H_3O^+$) and m/z 44, and exhibited a notably higher signal at m/z 29 (mainly CHO^+) than other OA factors, consistent with previous reports (Sun et al., 2016a; Xu et al., 2019; Zhao et al., 2019; Zhong et al., 2021). Moreover, BBOA correlated strongly with m/z 60 (mainly $C_2H_4O_2^+$) and m/z 73 (Pearson's r^2 (r^2) = 0.85, 0.80, $p < 0.001$); CCOA was strongly correlated with Chl and m/z 115 (r^2 = 0.56, 0.48, $p < 0.001$); HOA correlated with NO_2 and m/z 41 (r^2 = 0.47, 0.59, $p < 0.001$); and OOA and aqSOA were significantly correlated with NO_3/NH_4 (r^2 = 0.77, 0.75, $p < 0.001$) and SO_4/ALWC (r^2 = 0.67, 0.85, $p < 0.001$), respectively (Fig. S10). These results confirm the robustness and physicochemical plausibility of the five OA factors identified in this study. Overall, the average concentration of BBOA was 8.6 ± 7.7 μg m^{-3} and accounted for the

highest proportion of OA (34.8 ± 11.2%), followed by OOA (5.5 ± 3.5 μg m^{-3}, 21.7 ± 11.4%), CCOA (4.0 ± 3.3 μg m^{-3}, 15.7 ± 7.1%), HOA (3.5 ± 2.8 μg m^{-3}, 14.6 ± 8.1%), and aqSOA (3.3 ± 2.9 μg m^{-3}, 13.2 ± 5.9%) (Fig. 1). These results identified BBOA as the dominant component of OA in autumn in the SCB. Notably, the fraction of BBOA in OA in this study was much higher than those reported in wintertime studies in China (Table S1).

The contributions of BBOA and aqSOA to OA increased from CP (31.7% and 12.6%, respectively) to PP (38.6% and 14.1%, respectively), whereas those of CCOA, HOA, and OOA decreased. Significantly higher RH and ALWC were observed during PP (58.5 ± 12.4% and 69.4 ± 30.3 μg m^{-3}, respectively) than during CP (49.8 ± 8.9% and 37.1 ± 20.8 μg m^{-3}, respectively) ($p < 0.001$), whereas temperature showed no significant difference ($p > 0.1$). The average wind speed during CP was 1.3 times that during PP, reaching 0.32 ± 0.18 m s^{-1}. These results indicate that the atmosphere during PP was characterized by stagnation, higher RH, and elevated ALWC, likely leading to distinct sources and chemical processing of OA compared with CP.

Compared with CP, OA concentration exhibited an evident diurnal variation during PP. As shown in Fig. 2, the OA concentration peaked at 12:00 local time (LT) (82.7 μg m^{-3}) during daytime in PP, whereas in CP, the peak occurred at 21:00 LT. During PP, OA increased rapidly at a rate of 7.8 μg m^{-3} hr^{-1} from 09:00 to 12:00 LT, accompanied by a significant decrease in NO3. BBOA and aqSOA concentrations exhibited similar diurnal patterns to OA, with high values during daytime and a rapid increase from 09:00 to 12:00 LT during PP. Previous studies have indicated that the aqSOA mass spectrum showed a higher signal at m/z 29 (CHO^+) than other OA factors (Gilardoni et al., 2016; Meng et al., 2020; Wang et al., 2021). During PP, the tracer ion fragments for BBOA (m/z 60) and aqSOA (m/z 29) peaked at 12:00 LT (1.2 μg m^{-3}) and 13:00 LT (4.3 μg m^{-3}), respectively. Additionally, ALWC correlated more strongly with aqSOA concentration ($r^2 = 0.86$, $p < 0.001$) than with BBOA concentration ($r^2 = 0.58$, $p < 0.001$). Both ALWC and aqSOA concentrations peaked at 13:00 LT, later than the BBOA peak (12:00 LT), supporting that ALWC might play a significant role in the chemical processing that converts BBOA to aqSOA during PP.

In contrast, odd oxygen ($O_x = O_3 + NO_2$) showed weak correlations with both OOA and aqSOA concentrations throughout the campaign ($p > 0.1$, data not shown). Although the average O_x concentration was higher during PP (51.1 ± 19.6 ppb) than during CP (36.9 ± 14.0 ppb), no significant correlation was observed in either period. These results suggest that gas-phase photochemical oxidation might played a limited role in SOA formation in this study.

In summary, these results suggest that OA was the dominant component of $PM_{2.5}$, especially during PP in the SCB. During PP, BBOA and aqSOA contributed significantly to the daytime increase in OA concentration. Previous studies have shown that the autumn harvest period—specifically October and November—is characterized by intensified biomass burning in the SCB, primarily due to post-harvest crop-residue burning (Chen et al., 2017; Tao et al., 2014). Thus, daytime aqSOA formation during PP might be related to high aerosol water content and BBOA emissions (Bao et al., 2023; Chen et al., 2017; Chen et al., 2019; Tao et al., 2014). Additionally, Gilardoni et al. (2016) found that aqSOA, such as guaiacol dimer ($C_{14}H_{14}O_4^+$), could be formed from aged biomass-burning emissions in both fog water and wet aerosol, especially under high ALWC conditions. To further explore the formation of aqSOA from biomass-burning emissions through aqueous-phase reactions, the next section discusses the dynamic evolution of aqSOA in relation to BBOA.

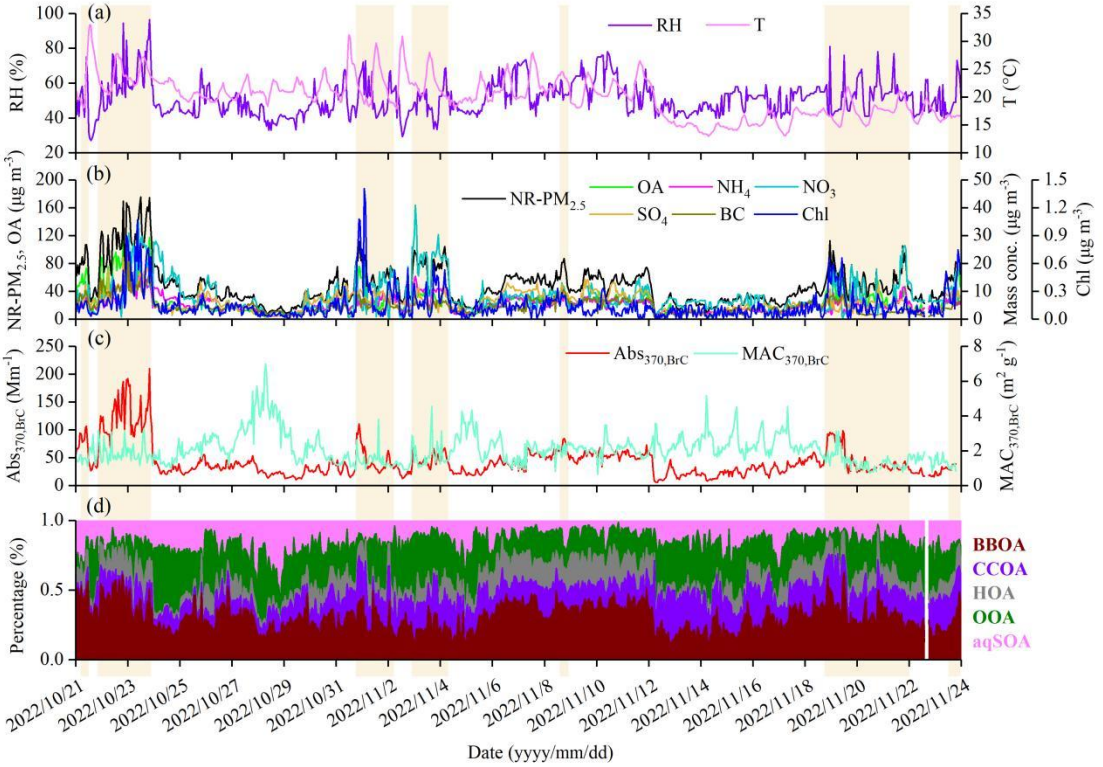

Figure 1. Time series of **(a)** RH and T, **(b)** NR-$PM_{2.5}$ species measured by the ToF-ACSM and BC, **(c)** $Abs_{370,BrC}$ and $MAC_{370,BrC}$, and **(d)** mass fractions of OA factors during the campaign. The pollution period (BC + NR-$PM_{2.5}$ > 75 μg m^{-3}) is highlighted by the shaded areas.

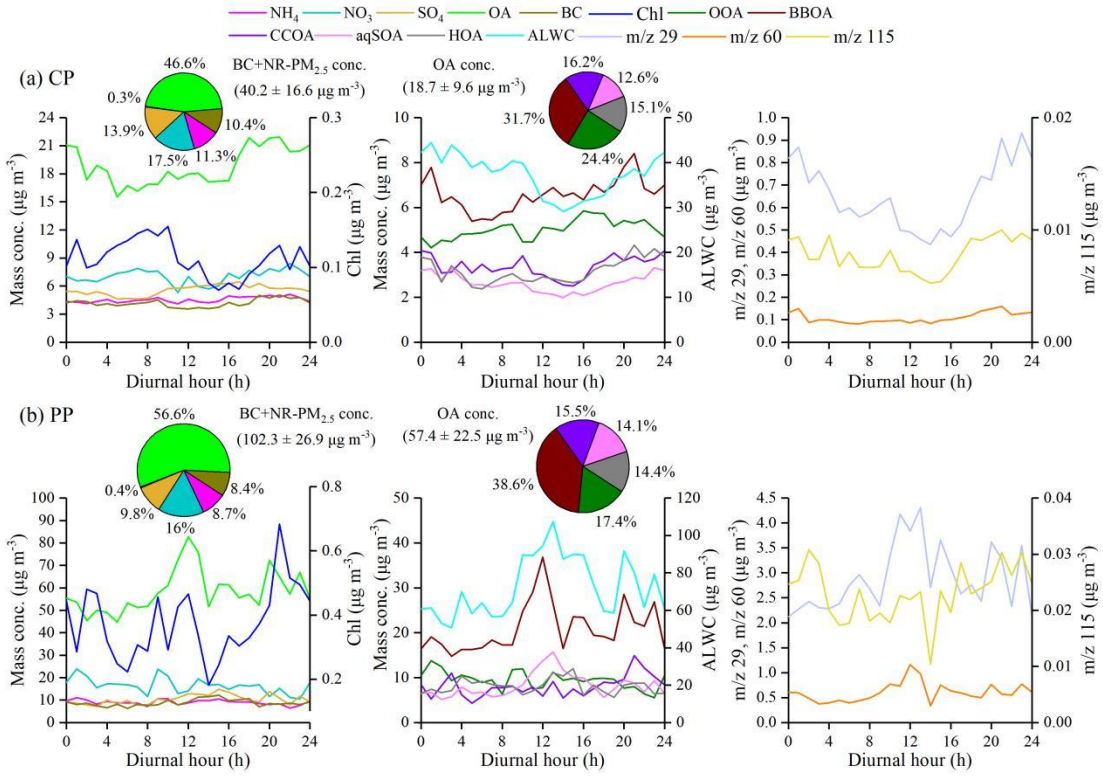

Figure 2. Diurnal variations of $PM_{2.5}$ species, BC, OA factors, m/z 29, m/z 60, and m/z 115 mass

concentrations during the **(a)** clean period (CP) (BC + NR-$PM_{2.5}$ < 75 μg m^{-3}) and **(b)** pollution period (PP) (BC + NR-$PM_{2.5}$ > 75 μg m^{-3}). The pie charts on the left side of panels **(a)** and **(b)** show the average mass contributions of different chemical compositions to BC + NR-$PM_{2.5}$ during CP and PP, respectively. Meanwhile, the average mass contributions of OOA, BBOA, CCOA, aqSOA, and HOA to OA are shown in the pie charts in the middle of panels **(a)** and **(b)**, respectively.

3.2 Biomass-burning emissions as precursors for aqSOA

Figure 3 shows a strong positive correlation between the mass fraction (%) of aqSOA in total $PM_{2.5}$ and ALWC during the campaign (r^2 = 0.64, p < 0.001). The contribution of aqSOA increased with increasing f_{29} values (the normalized signal at m/z 29). Notably, the aqSOA factor showed significantly higher f_{29} and f_{60} values (0.167 and 0.011, respectively) than the OOA factor (0.017 and 0.002, respectively) (Fig. S9). Moreover, both aqSOA concentrations and f_{29} were strongly correlated with ALWC (r^2 = 0.85, 0.73, p < 0.001) (Fig. 3). The average oxygen-to-carbon ratio (O:C) of the aqSOA factor (0.85) was 2.7 times that of the BBOA factor (0.31), whereas the hydrogen-to-carbon (H:C) ratios were similar (1.74 for aqSOA and 1.81 for BBOA), indicating the replacement of a hydrogen atom by an OH moiety (Lim et al., 2010; Ng et al., 2011a). These results were similar to aqSOA results in Italy and Beijing (Gilardoni et al., 2016; Zhao et al., 2019).

Previous studies indicate that aqueous-phase processes contribute to SOA formation from fossil fuel emissions (Ervens et al., 2011; Huang et al., 2023; Wang et al., 2021; Xu et al., 2022; Yan et al., 2017). Wang et al. (2021) and Xu et al. (2022) have highlighted the role of aqueous-phase reactions in SOA formation, particularly in regions with substantial anthropogenic emissions. In this study, a strong anticorrelation was observed between the mass fraction of fossil-fuel-related OA components (sum of CCOA, HOA and OOA) and ALWC at high f_{29} values (r^2 = 0.48, p < 0.001, data not shown), consistent with recent findings (Wang et al., 2021). This indicates that aqSOA may also be produced by aqueous-phase reactions of

fossil-fuel-related OA components.

Figure 4 shows the relationships between ALWC and the concentrations of OA factors as well as f_{29} during the campaign. The mass concentrations of all five resolved OA factors increased with increasing ALWC. However, compared with other OA factors, aqSOA and BBOA increased more significantly, from 1.1 and 4.9 μg m^{-3} to 5.2 and 10.8 μg m^{-3}, respectively, when 20 μg m^{-3} < ALWC < 60 μg m^{-3}. Notably, only the aqSOA concentration continued to rise under high ALWC conditions (> 100 μg m^{-3}). This enhancement likely resulted from the formation of more water-soluble organic species, such as glyoxal and methylglyoxal, which were subsequently oxidized to aqSOA via aqueous-phase reactions in aerosol liquid water (Carlton et al., 2007; Ervens et al., 2011; Tan et al., 2012).

As shown in Fig. 4b, the mass fraction of aqSOA increased significantly from 5% at ALWC < 20 μg m^{-3} to 17−22% at ALWC > 60 μg m^{-3}, accompanied by a corresponding decrease in the OOA fraction. In contrast, the contributions of POA (BBOA + CCOA + HOA) and SOA (OOA + aqSOA) remained relatively stable across different ALWC levels (58−68% and 32−42% for POA and SOA, respectively). This result suggests aqSOA forms more intensively than OOA through aqueous-phase reactions, although it may also be formed from OOA, consistent with recent studies in northwestern China (Zhao et al., 2019; Zhong et al., 2021).

Furthermore, f_{29} (CHO^+) increased from 0.010 to 0.227 as a function of ALWC (Fig. 4b). A pronounced rise in f_{29} from 0.055 to 0.210 occurred when ALWC increased from 60 μg m^{-3} to 100 μg m^{-3} ($p < 0.001$), tracking the concurrent increase in OA mass concentrations (13.2−109.1 μg m^{-3}). Previous laboratory analyses of organic standards have found that species without alcohol groups showed low f_{29} (< 0.05), while polyols and species with non-acid OH groups, which are common products of biomass-burning emissions, displayed high f_{29} values (0.05–0.15) (Canagaratna et al., 2015; Gilardoni et al., 2016; Zhao et al., 2014). This further supports the potential formation of organic compounds with hydroxyl groups, such as glyoxal and methylglyoxal, under high ALWC conditions. Overall, these results demonstrate that the observed aqSOA could be formed predominantly from

biomass-burning emissions through aqueous-phase reactions, reinforcing the important role of BBOA in increasing $PM_{2.5}$ mass concentration.

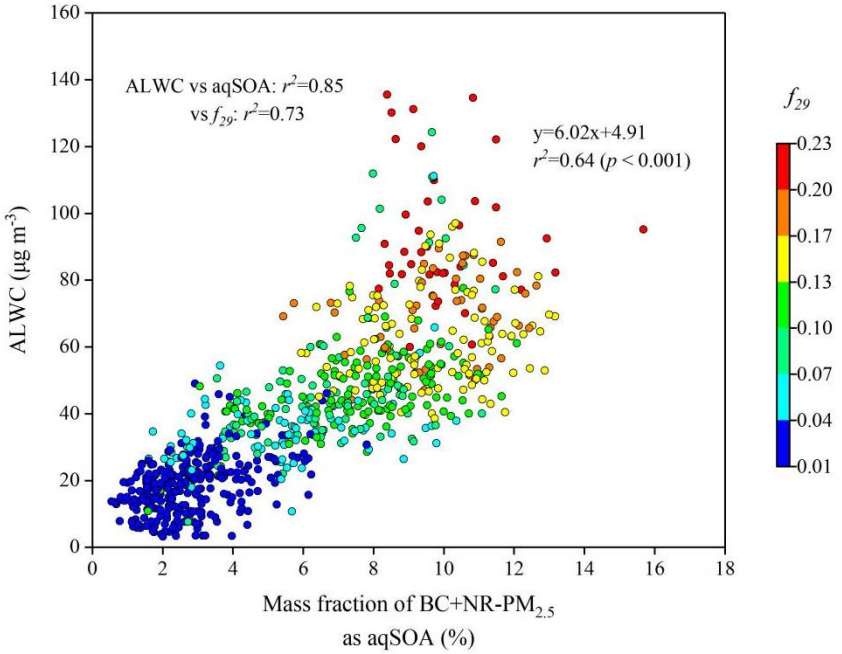

Figure 3. Scatter plot of the mass fraction of aqSOA in BC + NR-$PM_{2.5}$ versus ALWC, coloured by f_{29} (normalized signal at m/z 29) during the campaign. f_{29} (mainly CHO^+) is a tracer for alcohol compounds and is used to monitor the aqueous-phase oxidation of organic compounds, such as glyoxal.

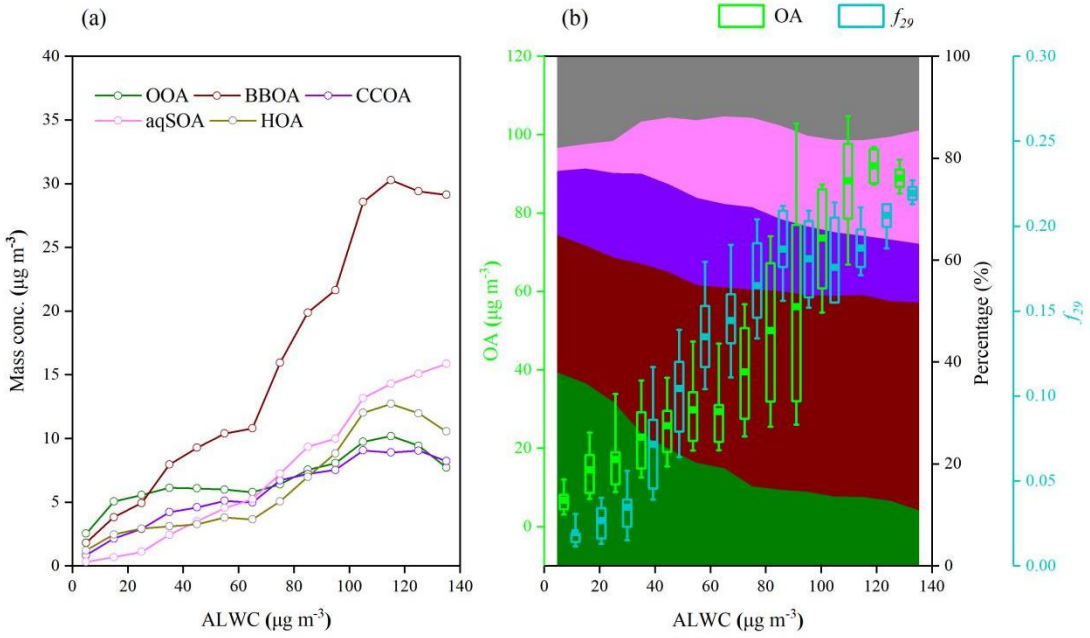

Figure 4. Variations of **(a)** OA factor mass concentrations, **(b)** OA mass concentrations, f_{29} (a tracer for alcohol compounds), and mass fraction of OA factors as a function of ALWC. Data were

grouped into different bins according to a 10-μg m^{-3} increment of ALWC.

To identify the formation of aqSOA and its precursors under different $PM_{2.5}$ pollution levels, the relationships between aqSOA and BBOA or OOA mass concentrations, as well as key ion-fragment tracers, were analyzed separately during CP and PP. The correlation (r^2) between aqSOA and BBOA was stronger during PP (0.64) than during CP (0.54) ($p < 0.001$, Fig. 5a, c). Although both aqSOA and BBOA concentrations increased with increasing ALWC during both periods, the correlations of ALWC with aqSOA and BBOA were relatively stronger during PP than during CP ($p < 0.001$). As shown in Fig. 5b, d, f_{29} was highly correlated with aqSOA formation during both CP and PP. A subset of data points with high aqSOA and OOA concentrations displayed relatively low f_{29} values (0.071−0.102), as shown in Fig. 5d. For these points, the average value of f_{44} (normalized signal of m/z 44) (0.103 ± 0.024) was 1.3 times that of the overall dataset (0.080 ± 0.035) during PP, likely due to the formation of more-oxidized OOA under high ALWC values (> 80 μg m^{-3}) (Xu et al., 2017). Previous studies have found that f_{29} values for polyols and species with non-acid OH groups from biomass-burning emissions were typically lower than 0.15 (Canagaratna et al., 2015; Gilardoni et al., 2016; Zhao et al., 2014). Moreover, the mass fraction of aqSOA showed a stable increasing trend and remained elevated (from 18% to 22%) at ALWC > 80 μg m^{-3}, accompanied by a corresponding decrease in OOA (from 15% to 10%) (Fig. 4b). In contrast to OOA ($p > 0.1$), aqSOA concentration showed a strong positive correlation with ALWC ($r^2 = 0.73$, $p < 0.001$) when ALWC > 80 μg m^{-3} during PP. However, no such correlations were observed during CP ($p > 0.1$). Notably, a strong anticorrelation between aqSOA and OOA concentrations was observed during PP at ALWC > 80 μg m^{-3} when $f_{29} > 0.15$ ($r^2 = 0.76$, $p < 0.001$), but not during CP ($p > 0.1$) (Fig. 5b, d). These results indicated that aqSOA formation was more intensive than OOA at high ALWC levels during PP.

Previous research demonstrated that f_{44} could be used as a tracer for aged SOA, f_{43} (normalized signal at m/z 43) for POA and fresh SOA, and f_{60} (presence of anhydrosugars) for BBOA (Cubison et al., 2011; Ng et al., 2010). Additionally, m/z 44 and 43 are typically from different functional groups, and their ratio changes as a

function of atmospheric aging. The triangle plot of f_{44} versus f_{43} has been widely used to characterize OA evolution, whereas that of f_{44} versus f_{60} is commonly used to track the aging of BBOA (Ortega et al., 2013; Paglione et al., 2020; Xu et al., 2017; Xu et al., 2019). In this study, the bottom region of the triangle (Fig. 6) was dominated by BBOA, CCOA, and HOA, which exhibited low f_{44} (0.040, 0.017, and 0.016, respectively), indicating fresh, less-oxidized emissions. In contrast, the f_{44} of SOA factors (OOA and aqSOA; 0.118 and 0.117, respectively) were observably higher, reflecting their oxidized nature. The f_{44} of aqSOA was close to that observed in fog (Gilardoni et al., 2016; Kim et al., 2019), highlighting the role of aqueous-phase reactions in this study. Moreover, the relative abundance of m/z 45 (mainly HCO_2^+), a tracer ion for carboxylic acids, was higher in the aqSOA spectrum than in the OOA spectrum (Fig. S9), consistent with previous findings that aqueous-phase reactions are important sources of oxygenated organic compounds, including organic acids (Ervens et al., 2011; Kim et al., 2019; McNeill, 2015; Sun et al., 2010; Yu et al., 2014). As shown in Fig. 6b, BBOA and aqSOA displayed higher f_{60} values (0.019 and 0.011, respectively) than CCOA (0.009) and HOA (0.008). The f_{60} value of OOA was 0.002, which is lower than the typical background level (0.003) observed in the atmosphere unaffected by biomass burning (Cubison et al., 2011). The mass spectrometry feature of aqSOA, characterized by elevated f_{44} and f_{60} values, placed it in the schematic region of aged BBOA reported in previous studies (Cubison et al., 2011; Ortega et al., 2013). Additionally, BBOA contains abundant water-soluble organic compounds, such as sugars, phenols, and organic acids, that can efficiently form aqSOA through aqueous-phase reactions, such as oxidation and oligomerization reactions (Ervens et al., 2011; Gilardoni et al., 2016; Lee et al., 2013; Lei et al., 2024; Li et al., 2020; Powelson et al., 2014). In contrast, OOA formation primarily relies on the gas-phase oxidation of VOCs with high-reactivity, such as aromatics and long-chain alkanes, by OH radicals, which have low concentrations in BBOA plumes (Akagi et al., 2011; Jimenez et al., 2009; Shrivastava et al., 2017; Yokelson et al., 2007). This suggests that BBOA acts as an important precursor for aqSOA instead of OOA through aqueous-phase reactions. These results are consistent with previous studies, and most

of the observed data fall within the triangle space (Bao et al., 2023; Kim et al., 2019; Paglione et al., 2020). Notably, aqSOA formation processes can be more intense and significant during autumn due to elevated precursor concentrations (e.g., BBOA), ALWC, and RH values, though the underlying chemical pathways are robust and can occur year-round (Bao et al., 2023; Tang et al., 2025; Zeng et al., 2025).

During PP, f_{44} values ranging from 0.022 to 0.140 (0.080 ± 0.035) were significantly higher than those during CP (0.021−0.150, 0.064 ± 0.019) ($p < 0.001$), whereas f_{43} was slightly lower, with an average of 0.062 ± 0.027. Compared with CP ($r^2 = 0.17$, slope = −0.53), f_{44} showed a more pronounced inverse relationship with f_{43} during PP, characterized by a higher r^2 value (0.70) and a regression slope closer to −1 (−1.09). This pattern indicated a greater abundance of aged SOA in the atmosphere during PP (Fig. 6a and c). Notably, data points in the $f_{44} - f_{43}$ space during PP fell within the upper boundary of the triangle region, with most points located outside the bottom boundary. These results suggested that less oxidized SOA was predominantly formed through aqueous-phase processing instead of gas-phase photochemical oxidation during PP (Kim et al., 2019; Zhao et al., 2019). Moreover, points outside the bottom boundary of the triangle region, characterized by higher f_{44} (> 0.05) and lower f_{43} (< 0.06), were associated with relatively higher ALWC during PP, a feature not observed during CP.

Here, the triangle plots of f_{44} versus f_{60}, coloured by ALWC under different $PM_{2.5}$ pollution levels, were analyzed (Fig. 6b, d), while the link between aqSOA and BBOA was further stressed by a schematic representation of aged BBOA. Except for a few outliers, f_{60} values were consistently higher than 0.003, and most data points fell within the triangular region, suggesting a widespread influence of biomass burning on OA. During PP, f_{60} ranged from 0.005 to 0.019 (0.010 ± 0.004), similar to the range observed in CP (from 0.004 to 0.019, 0.010 ± 0.003). However, the correlation between f_{44} and f_{60} was higher during PP ($r^2 = 0.72$) than during CP ($r^2 = 0.31$) ($p < 0.001$). Moreover, data points within the schematic space of aged BBOA showed relatively higher ALWC compared with the overall dataset during PP, a pattern that was not evident during CP.

Regional transport significantly influenced the aging of BBOA in the SCB. Previous studies have demonstrated that northeast winds prevail during autumn in this region, facilitating the transport of pollutants along the Dazhou→Guang'an→Hechuan pathway, and this northeast-southwest transport pathway had a significant impact on Chongqing (Peng et al., 2019; Wang et al., 2018). As shown in Fig. S11, air masses during the campaign predominantly originated from northeastern Chongqing, an area with widespread agricultural burning activities (He et al., 2015; Luo et al., 2020), and were transported over relatively short distances. Compared to other air mass clusters, the highest contribution and concentration of BBOA to total $PM_{2.5}$ were observed when air masses passed through northeastern Chongqing. The percentage of air mass trajectories that passed through biomass-burning-influenced regions was higher during PP (~57%) than during CP (~35%). Unlike Cluster 3 during CP, air masses originating from northeastern Chongqing (Cluster 2) during PP showed significantly higher contributions and concentrations of BBOA (24.7%, 27.8 μg m^{-3}) and aqSOA (9.4%, 10.6 μg m^{-3}) than other clusters ($p < 0.001$). In addition, Cluster 2 exhibited notably higher values of ALWC (93.7 μg m^{-3}), $Abs_{370,BrC,sec}$ (105.1 Mm^{-1}), f_{44} (0.113), and the NO_3/SO_4 ratio (2.1, a tracer for BBOA aging (Liu et al., 2024; Zhang et al., 2025)) than other clusters during PP ($p < 0.001$). During PP, approximately 68% of the trajectories in Cluster 2 passed through biomass-burning-influenced regions, with transport times to the sampling site ranging from 12 to 48 h, consistent with the typical timescale for aqueous-phase aging of biomass-burning emissions reported in earlier works (Cubison et al., 2011; Hennigan et al., 2010; Ortega et al., 2013; Zhu et al., 2023). These results suggest that regionally transported BBOA, primarily originating from northeastern Chongqing, underwent aging to form aqSOA within approximately 12–48 h.

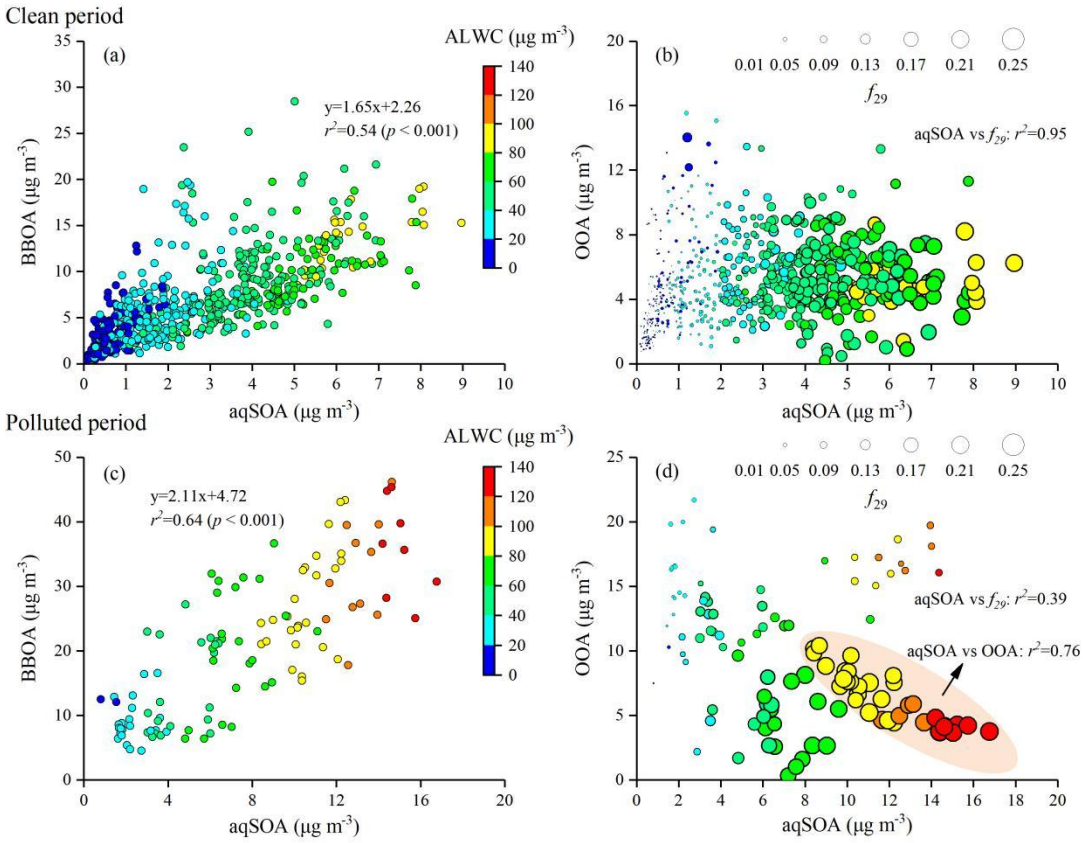

567

568 **Figure 5.** Scatter plots of aqSOA versus **(a, b)** BBOA and **(c, d)** OOA mass concentrations,
569 coloured by ALWC during CP and PP. The size of the symbols panel in **(b)** and **(d)** increases with
570 the increase in the f_{29} value, which is a tracer for alcohol compounds.

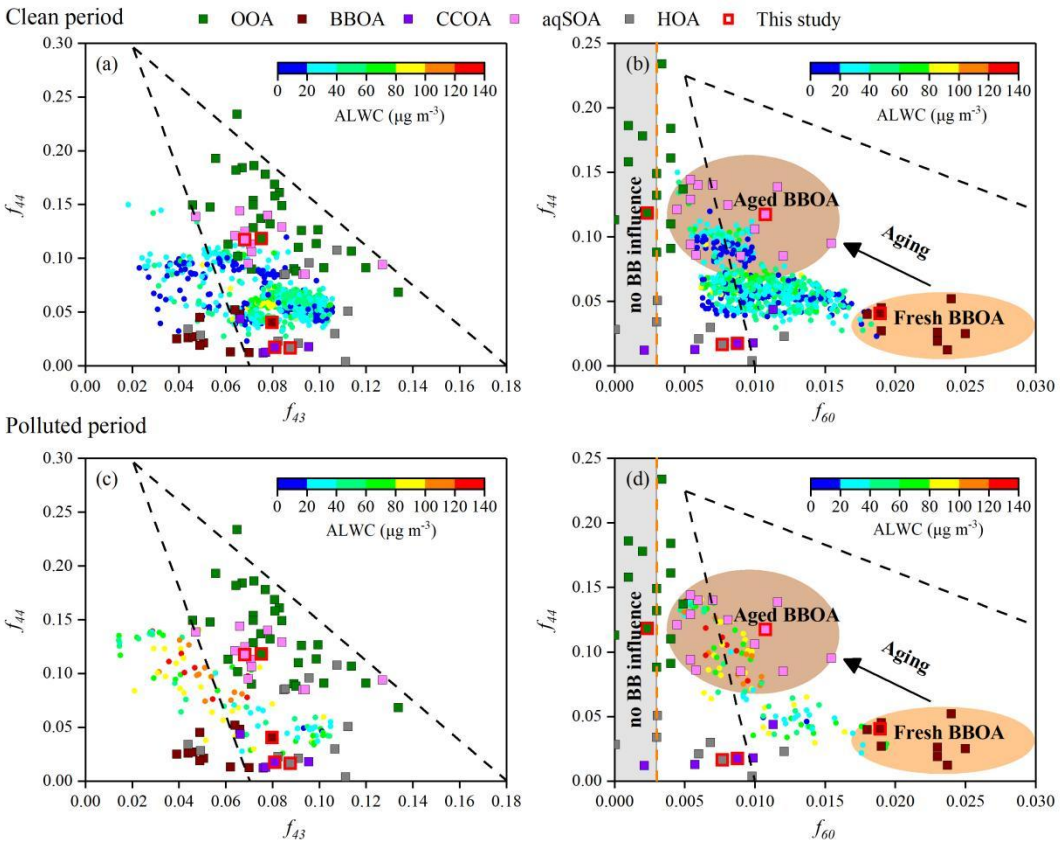

Figure 6. Triangle plots of **(a, c)** f_{44} (normalized mass spectrum signal at m/z 44) versus f_{43} (normalized mass spectrum signal at m/z 43) and **(b, d)** f_{44} versus f_{60} (normalized mass spectrum signal at m/z 60), coloured by ALWC (circles) during CP and PP. The dashed lines in **(a)** and **(c)** were derived from Ng et al. (2010) and used to follow the aging of OA components in the atmosphere. The background space (f_{60} < 0.003) without biomass burning influence is also shown by the grey shaded area. The background value of secondary aged OA (brown dashed line) and the black dashed lines characterizing the aging of BBOA in **(b)** and **(d)** were derived from Cubison et al. (2011). The data points (squares) included the measurements from this study (bordered in red) and previous research (Bao et al., 2023; Gilardoni et al., 2016; Kim et al., 2019; Ng et al., 2011a; Paglione et al., 2020; Xu et al., 2015; Xu et al., 2017; Xu et al., 2019; Zhao et al., 2017; Zhao et al., 2019). f_{43} (mainly $C_2H_3O^+$) is a tracer for POA and fresh SOA; f_{44} is a proxy of the OA oxygenation degree and used as a tracer for aged SOA; and f_{60} is a proxy of anhydrosugars emitted from biomass burning.

3.3 Evolution of BrC Absorption

Previous research indicates that OA from both fresh and aged biomass-burning emissions exhibits light absorption across the UV–Vis range, with significantly higher AAE values than BC, and may contribute to net positive radiative forcing (Laskin et al., 2015). In this study, the absorption properties of BrC and their relationships with the five OA factors were analyzed. The values of $Abs_{\lambda,BrC,pri}$ and $Abs_{\lambda,BrC,sec}$ were obtained using the MRS method, and the Abs value of each OA factor at each wavelength was estimated using the MLR method (SI Text S3 and S4). The mean $Abs_{370,BrC}$ was 42.4 ± 28.5 Mm^{-1} (accounting for 49.2% of Abs_{370}), much higher than $Abs_{660,BrC}$ (2.6 ± 1.3 Mm^{-1}, 10.5%), suggesting high absorption efficiency for BrC in the near-UV region. From 370 to 660 nm, $Abs_{\lambda,BrC,pri}$ and $Abs_{\lambda,BrC,sec}$ accounted for 56.8%−72.5% and 27.5%−43.2% of $Abs_{\lambda,BrC}$, respectively, indicating that primary emissions were the dominant contributors to BrC absorption (Fig. S13). However, the contribution of $Abs_{\lambda,BrC,sec}$ to $Abs_{\lambda,BrC}$ increased with wavelength, suggesting that the impact of SOA on Abs_{BrC} should not be ignored. The following analysis demonstrates that aqSOA formed from aged BBOA contributed substantially to the BrC budget and exhibited strong light absorption across the UV–Vis range.

Data at 370 nm, which exhibit higher SNRs and a greater contribution of Abs_{BrC}, were selected to further analyze the correlations of BrC absorption with various OA components. As described in Section 2.3.3, the Abs of the five OA factors at each wavelength were obtained using the MLR method (Table S2). The contributions of BBOA ($Abs_{370,BBOA}$) and aqSOA ($Abs_{370,aqSOA}$) to $Abs_{370,BrC}$ were 51.9% and 16.4%, respectively, exceeding those of CCOA (11.5%), HOA (9.1%), and OOA (11.1%). This pattern is consistent with the higher MAC values of BBOA and aqSOA (Fig. S15).

Figure S16 presents correlations between $Abs_{370,BrC}$ and the mass concentrations of OOA, BBOA, CCOOA, aqSOA, HOA, and the tracer ion m/z 60 (ion fragment tracers of BBOA). $Abs_{370,BrC}$ exhibited the strongest positive correlations with BBOA and m/z 60 (r^2 = 0.77, p < 0.001), followed by aqSOA (r^2 = 0.69, p < 0.001). In

contrast, correlations with HOA (r^2 = 0.36), CCOA (r^2 = 0.25), and OOA (r^2 = 0.09, p > 0.1) were much weaker. Among all OA factors (excluding BBOA), aqSOA contributed relatively more to $Abs_{370,BrC}$ (Table S2) and also displayed a stronger correlation with $Abs_{370,BrC}$. These results may be related to the formation of aqSOA from aged BBOA via aqueous-phase reactions. Gilardoni et al. (2016) demonstrated that aqSOA derived from aged BBOA through aqueous-phase reactions. Gilardoni et al. (2016) demonstrated that aqSOA derived from aged BBOA through aqueous-phase reactions in the ambient atmosphere contributes to the BrC budget and exhibits slightly higher $AAE_{467–660}$ (AAE of aerosols from 467 to 660 nm) values than fresh or processed biomass-burning emissions in laboratory experiments.

The MAC values of the five resolved OA components (equivalent to coefficients a–e in the MLR method) at different wavelengths are shown in Fig. S15. At 370 nm, BBOA showed the highest MAC (2.37 $m^2\ g^{-1}$), followed by aqSOA (1.23 $m^2\ g^{-1}$), indicating that oxidation of BBOA to aqSOA reduces light absorption at shorter wavelengths. Previous research found that the MAC of BBOA at 365 nm is twice that of SOA, which was associated with water-soluble BrC (Lorenzo et al., 2017; Washenfelder et al., 2015). The AAE values of the OA factors, calculated by a power-law fitting of their Abs from 370 nm to 660 nm (Qin et al., 2018; Wang et al., 2019b), are shown in Fig. S15. Notably, aqSOA had the lowest $AAE_{370–660,aqSOA}$ value (3.54), whereas BBOA had the highest $AAE_{370–660,BBOA}$ value (4.93). Moreover, the contribution of aqSOA to Abs_{BrC} increased from 16.4% at 370 nm to 26.7% at 660 nm, whereas that of BBOA decreased from 51.9% to 39.1% over the same wavelength range. These findings suggest that aqSOA formed from aged BBOA significantly contribute to the light absorption of BrC in the UV–Vis range.

Figure 7 shows a ternary contour map that quantifies the contributions of BBOA, CCOA, and HOA to $Abs_{370,BrC,pri}$. A strong positive correlation (p < 0.001) and a steep linear regression slope (1.80) were observed between the BBOA mass concentration and $Abs_{370,BrC,pri}$. Among these POA factors, high mass fractions of BBOA relative to POA were consistent with high values of $Abs_{370,BrC,pri}$ (Fig. 7a). For example, most data points with $Abs_{370,BrC,pri}$ higher than 49.1 Mm^{-1} (90th percentile of $Abs_{370,BrC}$) fell

within the region of high BBOA/POA values (> 0.5). Moreover, $Abs_{370,BrC,pri}$ increased significantly with increasing BBOA and m/z 60 mass concentrations, exhibiting higher correlation coefficients (r^2 = 0.63 and 0.55) than HOA (r^2 = 0.19) and CCOA (r^2 = 0.14) (Fig. 7b). These results indicate the major contribution of BBOA to primary BrC light absorption at 370 nm.

To understand the relationship between secondary BrC absorption and its chromophores, the correlation between $Abs_{370,BrC,sec}$ and the mass concentrations of SOA factors was analyzed. As shown in Fig. S17, $Abs_{370,BrC,sec}$ increased significantly with increasing aqSOA concentration (r^2 = 0.44, p < 0.001), and high $Abs_{370,BrC,sec}$ values were associated with elevated ALWC. In contrast, no such relationship was found for OOA (p > 0.1). The slope of the linear regression between aqSOA mass concentrations and $Abs_{370,BrC,sec}$ (3.50) was steeper than that for OOA (Fig. S17), and the MAC values of aqSOA were also higher across the UV–Vis range (Fig. S15).

To further characterize the evolution of secondary BrC absorption, $Abs_{370,BrC,sec}$ was normalized by ΔCO (background-corrected CO mixing ratios) to minimize the effect of boundary layer height (Fig. 8) (DeCarlo et al., 2010). Here, the background CO value (400 ppb) was defined as the lowest 1.25th percentile of CO values during the campaign (Kondo et al., 2006). Figure 8 shows that the ratios of $Abs_{370,BrC,sec}$/ΔCO increased with both aqSOA concentration and ALWC from 17:00 to 03:00 LT (r^2 = 0.63, 0.57, p < 0.001), whereas $Abs_{370,BrC,pri}$/ΔCO decreased slightly with increasing BBOA and m/z 60 concentrations over the same period (r^2 = 0.35, 0.33, p < 0.001). Additionally, the average concentrations of NO_3, NH_4, and NO_2 from 17:00 to 03:00 LT (9.1 μg m^{-3}, 5.6 μg m^{-3}, and 16.0 ppb, respectively) were 1.2, 1.2, and 1.3 times those from 04:00 to 16:00 LT (7.7 μg m^{-3}, 4.7 μg m^{-3}, and 12.6 ppb, respectively). These results are consistent with previous winter observations in the SCB (Peng et al., 2025; Wu et al., 2024).

As discussed in Section 3.2, SOA with hydroxyl groups, such as glyoxal and methylglyoxal, can form from aged BBOA through aqueous-phase reactions under high ALWC. Previous studies have shown that oligomers formed through aqueous reactions of glyoxal with NH_3, which contain C=C or C=N bonds, exhibit strong

absorption in near-UV regions (Laskin et al., 2015; Lee et al., 2013; Nozière et al., 2009; Powelsonet al., 2014). This suggested that secondary BrC chromophores with strong absorption at 370 nm were formed under high ALWC from 17:00 to 03:00 LT, which may be related to aqSOA generated from aged BBOA through aqueous-phase reactions. The low values of $Abs_{370,BrC,sec}/\Delta CO$ from 12:00 and 14:00 LT may be related to photolysis and/or photooxidation causing BrC photobleaching (Sareen et al., 2013; Zhao et al., 2015). Overall, our findings suggest that aqSOA formed from biomass-burning emissions contributed significantly to BrC absorption, especially at night during the campaign.

Previous studies indicate that biomass-burning activity is negligible in summer, and although it may also occur in spring and winter, its intensity is typically lower than in autumn (Chen et al., 2014; Chen et al., 2017; Tao et al., 2014; Yang et al., 2019). Tao et al. (2014) reported that biomass burning contributed 19 ± 11% to $PM_{2.5}$ during autumn, significantly higher than in other seasons, and accounted for the highest fraction of organic matter in $PM_{2.5}$. Additionally, the concentration of BBOA and its fraction in OA during autumn in this study (8.6 ± 7.7 μg m^{-3} and 34.8 ± 11.2%, respectively) were respectively higher than those observed during summer (0.41 μg m^{-3} and 5.7%, respectively) (Zeng et al., 2025) and winter in the SCB (Tang et al., 2025; Zhang et al., 2023) (Table S1). Notably, the ALWC during autumn in this study (41.6 ± 24.9 μg m^{-3}) was substantially higher than that reported for summer (18.6 ± 35.3 μg m^{-3}; Zeng et al., 2025) and winter (27.4 ± 9.7 μg m^{-3}; Tang et al., 2025) in the SCB. Wang et al. (2018) observed that RH values at Chengdu and Chongqing in autumn were also higher than those in other seasons. Previous research indicates that, while aqueous-chemistry pathways in spring were comparable to those in autumn, photochemical bleaching of BrC was potentially stronger in spring (Wang et al., 2019a). Although winter features lower biomass-burning emissions, secondary BrC could still form from BBOA through aqueous-phase reactions under high NO_x and NH_4 concentrations and stagnant nighttime conditions, as observed during winter in the SCB (Peng et al., 2025; Wu et al., 2024). In summer, elevated temperature and O_x ($O_x = NO_2 + O_3$) levels could enhance photochemical oxidation, promoting secondary

BrC formation while also intensifying BrC photobleaching (Wu et al., 2024). In summary, while secondary BrC can derive from BBOA through aqueous-phase reactions in all seasons in the SCB (with the possible exception of spring), the elevated ALWC and BBOA concentrations during autumn are favourable for its aqueous-phase formation.

$AAE_{370–880}$ is another key parameter for characterizing aerosol absorption properties. Figure 9 displays its correlations with the mass fraction of aqSOA (f_{aqSOA}) and BBOA (f_{BBOA}) to OA and the BC-to-OA ratio. During the campaign, a strong positive correlation ($r^2 = 0.49$, $p < 0.001$) was observed between $AAE_{370–880}$ and f_{aqSOA}, with $AAE_{370–880}$ reaching values up to 2.65. In contrast, $AAE_{370–880}$ increased only slightly with increasing f_{BBOA} ($r^2 = 0.21$, $p < 0.001$) (Fig. 9a, c). AAE was calculated using a power-law fitting of aerosol absorption values (Qin et al., 2018; Wang et al., 2019b). While BC concentration was linearly dependent on Abs_{BC}, OA concentration did not follow the same pattern with Abs_{BrC}. The mixing state of BC and OA, influenced by combustion conditions, can also affect AAE. Previous studies have shown that biomass-burning emissions can impact absorption properties, which is reflected in the relationship between AAE and the BC-to-OA ratio (a measure of the combustion conditions) (Lu et al., 2015; Saleh et al., 2014). Thus, the relationship observed in Fig. 9b reflects the influence of biomass-burning emissions during this campaign. The parameterised curve (black) agrees with prior research (red) for wavelengths from 370 to 880 nm (Lu et al., 2015). When 950 nm was used as the highest wavelength instead of 880 nm, $AAE_{370–950}$ values differed by less than 10% from $AAE_{370–880}$. Notably, data points with high $AAE_{370–880}$ corresponded to low BC-to-OA ratios and large f_{aqSOA} values. Moreover, the average value of $AAE_{370–880}$ observed in this study (1.95) was higher than $AAE_{370–950}$ observed in the laboratory experiments on fresh and photochemically aged biomass-burning emissions (i.e., 1.38 and 1.48 for fresh oak and pocosin pine, and 1.42 and 1.73 for aged oak and pocosin pine) (Saleh et al., 2013).

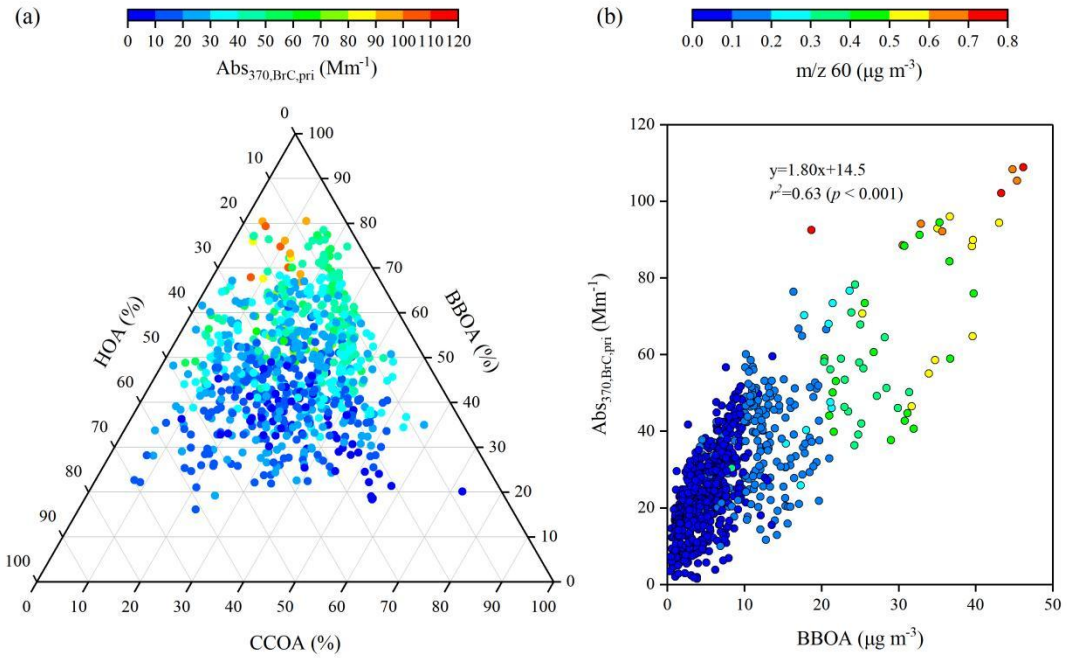

732

733 **Figure 7. (a)** Ternary diagram for the mass fractions of BBOA, CCOA, and HOA in POA,

734 coloured by $Abs_{370,BrC,pri}$, and **(b)** scatter plot of BBOA mass concentrations versus $Abs_{370,BrC,pri}$,

735 coloured by m/z 60 mass concentrations.

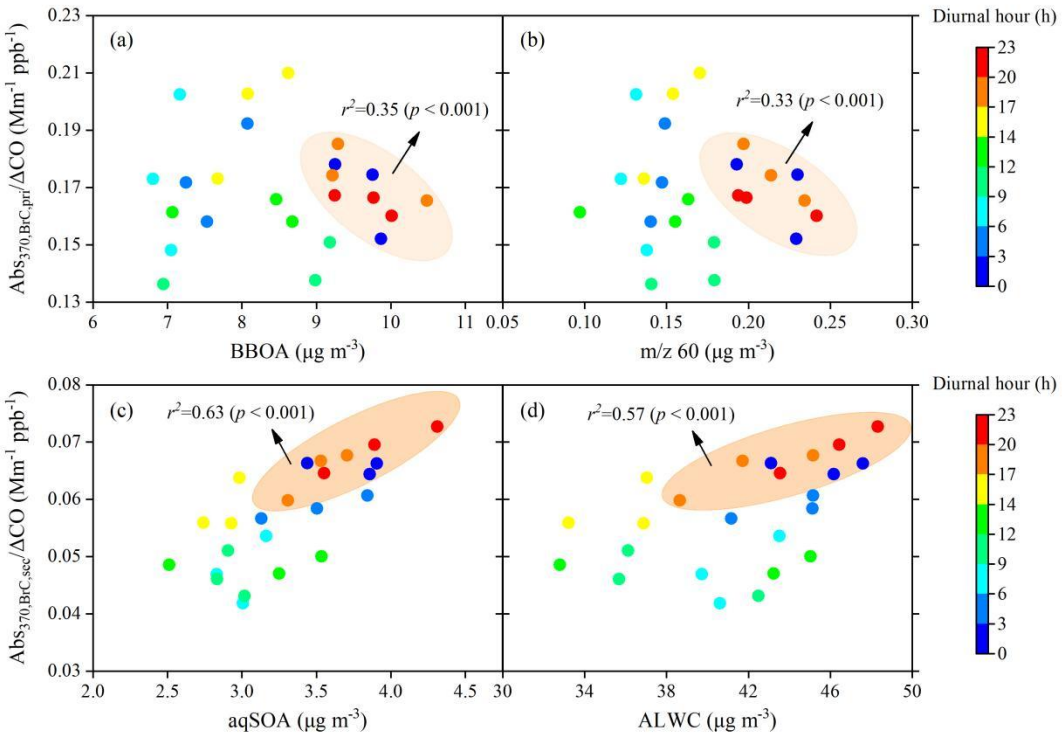

736

Figure 8. Scatter plots of $Abs_{370,BrC,pri}/\Delta CO$ versus **(a, b)** BBOA and m/z 60 mass concentrations and $Abs_{370,BrC,sec}/\Delta CO$ versus **(c, d)** aqSOA and ALWC, coloured by the local time.

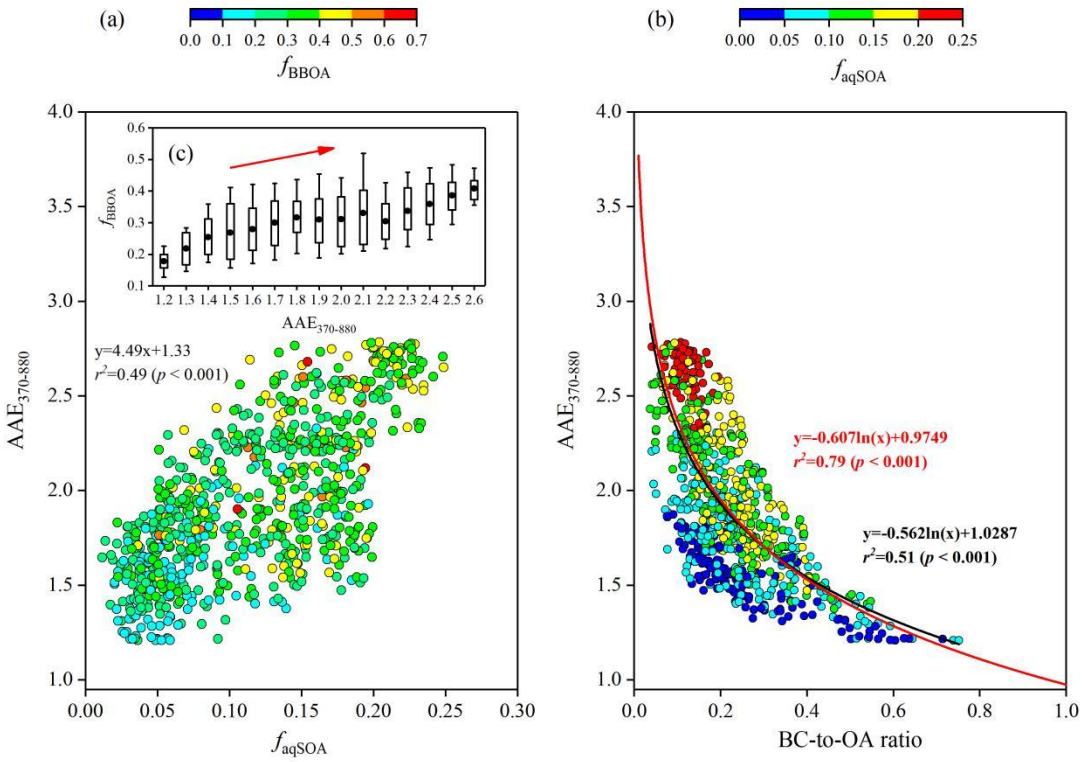

Figure 9. Relationship between **(a)** $AAE_{370–880}$ and the mass fraction of aqSOA (f_{aqSOA} = aqSOA/OA), coloured by the mass fraction of BBOA (f_{BBOA} = BBOA/OA), and **(b)** BC-to-OA ratios coloured by f_{aqSOA}. **(c)** Variations of f_{BBOA} as a function of $AAE_{370–880}$. The red curve in **(b)** was the best fit curve to data taken from Lu et al. (2015) and described the Abs of fresh and aged BBOA.

4 Conclusions

This study conducted comprehensive real-time measurements of the light absorption properties and chemical composition of carbonaceous aerosols during autumn in the Sichuan Basin, China. The findings demonstrated that aqueous secondary organic aerosol (aqSOA) formed from aged biomass-burning emissions under high aerosol liquid water content (ALWC > 60 μg m^{-3}) conditions significantly contributes to aerosol pollution and light absorption. OA was the dominant component

of $PM_{2.5}$ (46.6 ± 10.7%) and exhibited strong absorption at UV wavelengths ($Abs_{370,BrC}$ = 42.4 ± 28.5 Mm^{-1}). During PP, aqSOA contributed, on average, 14.1% to OA (7.6 μg m^{-3}), exhibiting enhanced oxidation (f_{29} = 0.141 ± 0.062, f_{44} = 0.080 ± 0.035) and substantial light absorption characteristics ($Abs_{370,BrC}$ = 91.6 Mm^{-1}, $AAE_{370–880}$ = 2.1). Additionally, less-oxidized aqSOA, formed predominantly through aqueous-phase reactions, instead of gas-phase photochemical oxidation of their precursors, significantly contributed to the dynamic evolution of haze pollution during PP. Backward trajectory analysis further revealed that regionally transported BBOA, which originated primarily from northeastern Chongqing, underwent aqueous-phase aging to aqSOA within approximately 12–48 h. These results underscore that aqueous-phase reactions of BBOA—particularly during the transport of biomass-burning plumes—convert primary emissions into strongly light-absorbing aqSOA, thereby substantially influencing regional haze formation and radiative forcing.

Our findings align with previous laboratory studies on biomass-burning BrC formation, and provide novel ambient quantification of these processes under realistic atmospheric conditions. The parameterized curve of $AAE_{370–880}$ versus BC-to-OA ratios in this study was consistent with previous laboratory research on biomass-burning emissions. The mean $AAE_{370–880}$ observed in this study (1.95) was higher than the values reported for fresh and photochemically aged biomass-burning emissions in laboratory experiments, and increased significantly with increasing f_{aqSOA} (r^2 = 0.49, p < 0.001). Additionally, elevated $Abs_{370,BrC,sec}$ values coincided with high ALWC, NO_3, and NH_4 levels and correlated strongly with aqSOA concentration (r^2 = 0.44, p < 0.001). These results suggest that aqueous-phase reactions of BBOA under high-NO_x and high-NH_4 conditions produce secondary BrC with particularly strong light absorption. Notably, seasonal variations in biomass-burning emissions and the associated chemical processing of carbonaceous aerosols must be adequately represented in climate and air quality models. Conducting the campaign in autumn, when biomass-burning activity is intense, is critical to avoid underestimating aerosol impacts in this season and overestimating them in other seasons. However, the results

may not fully represent aerosol processes in other seasons. The relative uncertainty of Abs_{BrC} at 370 nm, resulting from the choice of AAE_{BC}, ranged from −112% to 42%. Nevertheless, our results underscore the importance of aqueous-phase processing in transforming biomass-burning emissions, with important implications for climate and air quality modelling. The substantial contribution of aqSOA to aerosol mass and light absorption highlights the requirement for improved representation of aqueous processes in models. The linkages established here among aging timescales, transport pathways, and aqSOA formation provide a transferable framework for understanding aqSOA processing in other humid regions influenced by biomass burning. Research on BrC chromophores is still in its early stages, and quantitative linking their chemical composition and light absorption properties to biomass-burning emissions across different seasons are necessary to improve our understanding of their climatic and environmental effects. Future research should prioritize molecular-level characterization of aqSOA precursors and products, quantification of aqueous reaction rates under ambient conditions, and multi-scale modelling to assess regional climate impacts. This study highlights that aqueous processes play an important role in the evolution of biomass-burning emissions and should be adequately considered in both air quality budgets and climate forcing balance on a global scale.

Data availability. The data generated and analysed in this study are available from https://doi.org/10.5281/zenodo.18635386 (Peng et al., 2026).

Author contributions. CZ, CP, YD, and ZL designed the experiments. Data analysis and interpretation were performed by CP, ZT, HT, KZ, ZL, and GS. CP, XY, and MT wrote the paper. ZT, YC, XL, LZ, YC, and YF contributed to the paper with useful scientific discussions or comments.

Competing interests. The authors declare that they have no conflict of interest.

Acknowledgements. This study was supported by the National Natural Science

Foundation of China (No. 42305126), National Key Research and Development Program of China (No. 2023YFC3709301), Natural Science Foundation of Chongqing Municipality (No. CSTB2022NSCQ-MSX0504).

References

Akagi, S. K., Yokelson, R. J., Wiedinmyer, C., Alvarado, M. J., Reid, J. S., Karl, T., Crounse, J. D., and Wennberg, P. O.: Emission factors for open and domestic biomass burning for use in atmospheric models, Atmos. Chem. Phys., 11, 4039−4072, https://doi.org/10.5194/acp-11-4039-2011, 2011.

Alfarra, M. R., Prévôt, A. S. H., Szidat, S., Sandradewi, J., Sandradewi, S., Lanz, V. A., Schreiber, D., Mohr, M., and Baltensperger, U.: Identification of the Mass Spectral Signature of Organic Aerosols from Wood Burning Emissions, Environ. Sci. Technol., 41, 5770−5777, https://doi.org/10.1021/es062289b, 2007.

Bahreini, R., Ervens, B., Middlebrook, A. M., Warneke, C., de Gouw, J. A., DeCarlo, P. F., Jimenez, J. L., Brock, C. A., Neuman, J. A., Ryerson, T. B., Stark, H., Atlas, E., Brioude, J., Fried, A., Holloway, J. S., Peischl, J., Richter, D., Walega, J., Weibring, P., Wollny, A. G., and Fehsenfeld, F. C.: Organic Aerosol Formation in Urban and Industrial Plumes Near Houston and Dallas, Texas, J. Geophys. Res.: Atmos., 114, D00F16, doi:10.1029/2008JD011493, 2009.

Bao, Z. E., Liu, Y. L., Meng, L. S., Han, Y., Tian, M., Shi, G. M., Wang, Q. Y., Huang, Y., Peng, C., Luo, B., Zhang, W., Wang, H. B., Cao, J. J., Yang, F. M., and Chen, Y.: Evaluating the effects of biomass burning on severe haze formation in a megacity of Sichuan Basin, Southwestern China, J. Geophys. Res.: Atmos., 130, e2024JD042516, https://doi.org/10.1029/ 2024JD042516, 2025.

Bao, Z. E., Zeng, X. L., Zhou, J. W., Yang, F. M., Lu, K. D., Zhai, C. Z., Li, X., Feng, M., Tan, Q. W., and Chen, Y.: Evolution of black carbon and brown carbon during summertime in Southwestern China: An assessment of control measures during the 2023 Chengdu Summer World University Games, Environ. Pollut., 357, 124467, https://doi.org/10.1016/j.envpol.2024.124467, 2024.

Bao, Z. E., Zhang, X. Y., Li, Q., Zhou, J. W., Shi, G. M., Zhou, L., Yang, F. M., Xie, S. D., Zhang, D., Zhai, C. Z., Li, Z. L., Peng, C., and Chen, Y.: Measurement report: Intensive biomass burning emissions and rapid nitrate formation drive severe haze formation in the Sichuan Basin, China – insights from aerosol mass spectrometry, Atmos. Chem. Phys., 23, 1147−1167, https://doi.org/10.5194/acp-23-1147-2023,

2023.

Canagaratna, M. R., Jayne, J. T., Jimenez, J. L., Allan, J. D., Alfarra, M. R., Zhang, Q., Onasch, T. B., Drewnick, F., Coe, H., Middlebrook, A., Delia, A., Williams, L. R., Trimborn, A. M., Northway, M. J., DeCarlo, P. F., Kolb, C. E., Davidovits, P., and Worsnop, D. R.: Chemical and microphysical characterization of ambient aerosols with the aerodyne aerosol mass spectrometer, Mass Spectrom. Rev., 26, 185−222, https://doi.org/10.1002/mas.20115, 2007.

Canagaratna, M. R., Jimenez, J. L., Kroll, J. H., Chen, Q., Kessler, S. H., Massoli, P., Hildebrandt Ruiz, L., Fortner, E., Williams, L. R., Wilson, K. R., Surratt, J. D., Donahue, N. M., Jayne, J. T., and Worsnop, D. R.: Elemental ratio measurements of organic compounds using aerosol mass spectrometry: characterization, improved calibration, and implications, Atmos. Chem. Phys., 15, 253−272, https://doi.org/10.5194/acp-15-253-2015, 2015.

Canonaco, F., Crippa, M., Slowik, J. G., Baltensperger, U., and Prévôt, A. S. H.: SoFi, an IGOR-based interface for the efficient use of the generalized multilinear engine (ME-2) for the source apportionment: ME-2 application to aerosol mass spectrometer data, Atmos. Meas. Tech., 6, 3649−3661, https://doi.org/10.5194/amt-6-3649-2013, 2013.

Carlton, A. G., Turpin, B. J., Altieri, K. E., Seitzinger, S., Reff, A., Lim, H. J., and Ervens, B.: Atmospheric oxalic acid and SOA production from glyoxal: results of aqueous photooxidation experiments, Atmos. Environ., 41, 7588−7602, https://doi.org/10.1016/j.atmosenv.2007.05.035, 2007.

Chen, C. R., Zhang, H. X., Yan, W. J., Wu, N. N., Zhang, Q., and He, K. B.: Aerosol water content enhancement leads to changes in the major formation mechanisms of nitrate and secondary organic aerosols in winter over the North China Plain, Environ. Pollut., 287, 117625, https://doi.org/10.1016/j.envpol.2021.117625, 2021.

Chen, Y., Tian, M., Huang, R. J., Shi, G. M., Wang, H. B., Peng, C., Cao, J. J., Wang, Q. Y., Zhang, S. M., Guo, D. M., Zhang, L. Y., and Yang, F. M.: Characterization of urban amine-containing particles in southwestern China: seasonal variation, source, and processing, Atmos. Chem. Phys., 19, 3245−3255,

https://doi.org/10.5194/acp-19-3245-2019, 2019.

Chen, Y., Xie, S. D., Luo, B., and Zhai, C. Z.: Characteristics and origins of carbonaceous aerosol in the Sichuan Basin, China, Atmos. Environ., 94, 215−223, https://doi.org/10.1016/j.atmosenv.2014.05.037, 2014.

Chen, Y., Xie, S. D., Luo, B., and Zhai, C. Z.: Particulate pollution in urban Chongqing of southwest China: Historical trends of variation, chemical characteristics and source apportionment, Sci. Total Environ., 584−585, 523−534, https://doi.org/10.1016/j.scitotenv.2017.01.060, 2017.

Coen, M. C., Weingartner, E., Apituley, A., Ceburnis, D., Fierz-Schmidhauser, R., Flentje, H., Henzing, J. S., Jennings, S. G., Moerman, M., Petzold, A., Schmid, O., and Baltensperger, U.: Minimizing light absorption measurement artifacts of the Aethalometer: Evaluation of five correction algorithms, Atmos. Meas. Tech., 3, 457−474, https://doi.org/10.5194/amt-3-457-2010, 2010.

Cubison, M. J., Ortega, A. M., Hayes, P. L., Farmer, D. K., Day, D., Lechner, M. J., Brune, W. H., Apel, E., Diskin, G. S., Fisher, J. A., Fuelberg, H. E., Hecobian, A., Knapp, D. J., Mikoviny, T., Riemer, D., Sachse, G. W., Sessions, W., Weber, R. J., Weinheimer, A. J., Wisthaler, A., and Jimenez, J. L.: Effects of aging on organic aerosol from open biomass burning smoke in aircraft and laboratory studies, Atmos. Chem. Phys., 11, 12049−12064, https://doi.org/10.5194/acp-11-12049-2011, 2011.

DeCarlo, P. F., Ulbrich, I. M., Crounse, J., de Foy, B., Dunlea, E. J., Aiken, A. C., Knapp, D., Weinheimer, A. J., Campos, T., Wennberg, P. O., and Jimenez, J. L.: Investigation of the Sources and Processing of Organic Aerosol over the Central Mexican Plateau from Aircraft Measurements during MILAGRO, Atmos. Chem. Phys., 10, 5257−5280, https://doi.org/10.5194/acp-10-5257-2010, 2010.

Drinovec, L., Močnik, G., Zotter, P., Prévôt, A. S. H., Ruckstuhl, C., Coz, E., Rupakheti, M., Sciare, J., Müller, T., Wiedensohler, A., and Hansen, A. D. A.: The "dual-spot" Aethalometer: an improved measurement of aerosol black carbon with real-time loading compensation, Atmos. Meas. Tech., 8, 1965−1979, https://doi.org/10.5194/amt-8-1965-2015, 2015.

Drozd, G. T. and McNeill, V. F.: Organic matrix effects on the formation of

light-absorbing compounds from α-dicarbonyls in aqueous salt solution, Environ. Sci.: Processes Impacts, 16, 741−747, https://doi.org/10.1039/c3em00579h, 2014.

Elser, M., Huang, R. J., Wolf, R., Slowik, J. G., Wang, Q. Y., Canonaco, F., Li, G. H., Bozzetti, C., Daellenbach, K. R., Huang, Y., Zhang, R. J., Li, Z. Q., Cao, J. J., Baltensperger, U., El-Haddad, I., and Prévôt, A. S. H.: New insights into $PM_{2.5}$ chemical composition and sources in two major cities in China during extreme haze events using aerosol mass spectrometry, Atmos. Chem. Phys., 16, 3207−3225, https://doi.org/10.5194/acp-16-3207-2016, 2016.

Ervens, B., Turpin, B. J., and Weber, R. J.: Secondary organic aerosol formation in cloud droplets and aqueous particles (aqSOA): a review of laboratory, field and model studies, Atmos. Chem. Phys., 11, 11069−11102, https://doi.org/10.5194/acp-11-11069-2011, 2011.

Feng, Z., Liu, Y., Zheng, F., Yan, C., Fu, P., Zhang, Y., Lian, C., Wang, W., Cai, J., Du, W., Chu, B., Wang, Y., Kangasluoma, J., Bianchi, F., Petäjä, T., and Kulmala, M.: Highly oxidized organic aerosols in Beijing: Possible contribution of aqueous-phase chemistry, Atmos. Environ., 273, 118971, https://doi.org/10.1016/j.atmosenv.2022.118971, 2022.

Fountoukis, C. and Nenes, A.: ISORROPIA II: a computationally efficient thermodynamic equilibrium model for K^+–Ca^{2+}–Mg^{2+}–NH_4^+–Na^+–SO_4^{2-}–NO_3^-–Cl^-–H_2O aerosols, Atmos. Chem. Phys., 7, 4639−4659, https://doi.org/10.5194/acp-7-4639-2007, 2007.

Fröhlich, R., Cubison, M. J., Slowik, J. G., Bukowiecki, N., Prévôt, A. S. H., Baltensperger, U., Schneider, J., Kimmel, J. R., Gonin, M., Rohner, U., Worsnop, D. R., and Jayne, J. T.: The ToF-ACSM: a portable aerosol chemical speciation monitor with TOFMS detection, Atmos. Meas. Tech., 6, 3225−3241, https://doi.org/10.5194/amt-6-3225-2013, 2013.

Gilardoni, S., Massoli, P., Paglione, M., Giulianelli, L., Carbone, C., Rinaldi, M., Decesari, S., Sandrini, S., Costabile, F., Gobbi, G. P., Pietrogrande, M. C., Visentin, M., Scotto, F., Fuzzi, S., and Facchini, M. C.: Direct observation of aqueous secondary organic aerosol from biomass-burning emissions, Proc. Natl. Acad. Sci.

935 USA, 113, 10013−10018, https://doi.org/10.1073/pnas.1602212113, 2016.
936 Guo, H. Y., Xu, L., Bougiatioti, A., Cerully, K. M., Capps, S. L., Hite Jr., J.R., Carlton,
937 A. G., Lee, S. H., Bergin, M. H., Ng, N. L., Nenes, A., and Weber, R. J.:
938 Fine-particle water and pH in the southeastern United States, Atmos. Chem. Phys.,
939 15, 5211−5228, https://doi.org/10.5194/acp-15-5211-2015, 2015.
940 Gyawali, M., Arnott, W. P., Lewis, K., and Moosmüller, H.: In situ aerosol optics in
941 Reno, NV, USA during and after the summer 2008 California wildfires and the
942 influence of absorbing and non-absorbing organic coatings on spectral light
943 absorption, Atmos. Chem. Phys., 9, 8007−8015,
944 https://doi.org/10.5194/acp-9-8007-2009, 2009.
945 He, M., Wang, X. R., Han, L., Feng, X. D., and M, X.: Emission Inventory of Crop
946 Residues Field Burning and Its Temporal and Spatial Distribution in Sichuan
947 Province, Environ. Sci., 36, 1208−1216,
948 https://doi.org/10.13227/j.hjkx.2015.04.010, 2015.
949 Hennigan, C. J., Izumi, J., Sullivan, A. P., Weber, R. J., and Nenes, A.: A critical
950 evaluation of proxy methods used to estimate the acidity of atmospheric particles,
951 Atmos. Chem. Phys., 15, 2775–2790, https://doi.org/10.5194/acp-15-2775-2015,
952 2015.
953 Hennigan, C. J., Sullivan, A. P., Collett, J. L., and Robinson, A. L.: Levoglucosan
954 stability in biomass burning particles exposed to hydroxyl radicals, Geophys. Res.
955 Lett., 37, L09806, https://doi.org/10.1029/2010GL043088, 2010.
956 Herrmann, H., Schaefer, T., Tilgner, A., Styler, S. A., Weller, C., Teich, M., and Otto,
957 T.: Tropospheric Aqueous-Phase Chemistry: Kinetics, Mechanisms, and Its
958 Coupling to a Changing Gas Phase, Chem. Rev., 115, 4259−4334,
959 https://doi.org/10.1021/cr500447k, 2015.
960 Huang, R. J., Zhang, Y. L., Bozzetti, C., Ho, K. F., Cao, J. J., Han, Y. M., Daellenbach,
961 K. R., Slowik, J. G., Platt, S. M., Canonaco, F., Zotter, P., Wolf, R., Pieber, S. M.,
962 Bruns, E. A., Crippa, M., Ciarelli, G., Piazzalunga, A., Schwikowski, M.,
963 Abbaszade, G., Schnelle-Kreis, J., Zimmermann, R., An, Z. S., Szidat, S.,
964 Baltensperger, U., El Haddad, I., and Prevot, A. S.: High secondary aerosol

965 contribution to particulate pollution during haze events in China, Nature, 514,
966 218−222, https://doi.org/10.1038/nature13774, 2014.
967 Huang, R. J., He, Y., Duan, J., Li, Y. J., Chen, Q., Zheng, Y., Chen, Y., Hu, W. W., Lin,
968 C. S., Ni, H. Y., Dai, W. T., Cao, J. J., Wu, Y. F., Zhang, R. J., Xu, W., Ovadnevaite,
969 J., Ceburnis, D., Hoffmann, T., and O'Dowd, C. D.: Contrasting sources and
970 processes of particulate species in haze days with low and high relative humidity in
971 wintertime Beijing, Atmos. Chem. Phys., 20, 9101−9114,
972 https://doi.org/10.5194/acp-20-9101-2020, 2020.
973 Huang, X. J., Liu, Z., Ge, Y. Z., Li, Q., Wang, X. F., Fu, H. B., Zhu, J., Zhou, B.,
974 Wang, L., George, C., Wang, Y., Wang, X. F., Su, J. X., Xue, L. K., Yu, S. C.,
975 Mellouki, A., and Chen, J. M.: Aerosol high water contents favor sulfate and
976 secondary organic aerosol formation from fossil fuel combustion emissions, npj
977 Clim. Atmos. Sci., 6, 173, https://doi.org/10.1038/s41612-023-00504-1, 2023.
978 Jimenez, J. L., Canagaratna, M. R., Donahue, N. M., Prevot, A. S. H., Zhang, Q.,
979 Kroll, J. H., DeCarlo, P. F., Allan, J. D., Coe, H., Ng, N. L., Aiken, A. C., Docherty,
980 K. S., Ulbrich, I. M., Grieshop, A. P., Robinson, A. L., Duplissy, J., Smith, J. D.,
981 Wilson, K. R., Lanz, V. A., Hueglin, C., Sun, Y. L., Tian, J., Laaksonen, A.,
982 Raatikainen, T., Rautiainen, J., Vaattovaara, P., Ehn, M., Kulmala, M., Tomlinson, J.
983 M., Collins, D. R., Cubison, M. J., Dunlea, J., Huffman, J. A., Onasch, T. B.,
984 Alfarra, M. R., Williams, P. I., Bower, K., Kondo, Y., Schneider, J., Drewnick, F.,
985 Borrmann, S., Weimer, S., Demerjian, K., Salcedo, D., Cottrell, L., Griffin, R.,
986 Takami, A., Miyoshi, T., Hatakeyama, S., Shimono, A., Sun, J. Y., Zhang, Y. M.,
987 Dzepina, K., Kimmel, J. R., Sueper, D., Jayne, J. T., Herndon, S. C., Trimborn, A.
988 M., Williams, L. R., Wood, E. C., Middlebrook, A. M., Kolb, C. E., Baltensperger,
989 U., and Worsnop, D. R.: Evolution of Organic Aerosols in the Atmosphere, Science,
990 326, 1525−1529, https://doi.org/10.1126/science.1180353, 2009.
991 Kampf, C. J., Jakob, R., and Hoffmann, T.: Identification and characterization of
992 aging products in the glyoxal/ammonium sulfate system – implications for
993 light-absorbing material in atmospheric aerosols, Atmos. Chem. Phys., 12,
994 6323−6333, https://doi.org/10.5194/acp-12-6323-2012, 2012.

995 Kim, H., Collier, S., Ge, X. L., Xu, J. Z., Sun, Y. L., Jiang, W. Q., Wang, Y. L.,
996 Herckes, P., and Zhang, Q.: Chemical processing of water-soluble species and
997 formation of secondary organic aerosol in fogs, Atmos. Environ., 200, 158−166,
998 https://doi.org/10.1016/j.atmosenv.2018.11.062, 2019.
999 Kirchstetter, T. W. and Novakov T.: Evidence that the spectral dependence of light
1000 absorption by aerosols is affected by organic carbon, J. Geophys. Res., 109,
1001 D21208, https://doi.org/10.1029/2004JD004999, 2004.
1002 Kondo, Y., Komazaki, Y., Miyazaki, Y., Moteki, N., Takegawa, N., Kodama, D.,
1003 Deguchi, S., Nogami, M., Fukuda, M., Miyakawa, T., Morino, Y., Koike, M.,
1004 Sakurai, H., and Ehara, K.: Temporal Variations of Elemental Carbon in Tokyo, J.
1005 Geophys. Res., 111, D12205, https://doi.org/10.1029/2005JD006257, 2006.
1006 Kourtchev, I., Giorio, C., Manninen, A., Wilson, E., Mahon, B., Aalto, J., Kajos, M.,
1007 Venables, D., Ruuskanen, T., Levula, J., Loponen, M., Connors, S., Harris, N.,
1008 Zhao, D. F., Kiendler-Scharr, A., Mentel, T., Rudich, Y., Hallquist, M., Doussin, J.
1009 F., Maenhaut, W., Bäck, J., Petäjä, T., Wenger, J., Kulmala, Ma., and Kalberer, M.:
1010 Enhanced Volatile Organic Compounds emissions and organic aerosol mass
1011 increase the oligomer content of atmospheric aerosols, Sci. Rep., 6, 35038,
1012 https://doi.org/10.1038/srep35038, 2016.
1013 Kroflic, A., Grilc, M., and Grgic, I.: Unraveling pathways of guaiacol nitration in
1014 atmospheric waters: nitrite, a source of reactive nitronium ion in the atmosphere,
1015 Environ. Sci. Technol., 49, 9150−9158, https://doi.org/10.1021/acs.est.5b01811,
1016 2015.
1017 Lack, D. A., and Langridge, J. M.: On the attribution of black and brown carbon light
1018 absorption using the Ångström exponent, Atmos. Chem. Phys., 13, 10535−10543,
1019 https://doi.org/10.5194/acp-13-10535-2013, 2013.
1020 Lanz, V. A., Alfarra, M. R., Baltensperger, U., Buchmann, B., Hueglin, C., and Prévôt,
1021 A. S. H.: Source apportionment of submicron organic aerosols at an urban site by
1022 factor analytical modelling of aerosol mass spectra, Atmos. Chem. Phys., 7,
1023 1503−1522, doi:10.5194/acp-7-1503-2007, 2007.
1024 Laskin, A., Laskin, J., and Nizkorodov, S. A.: Chemistry of atmospheric brown carbon,

Chem. Rev., 115, 4335−4382, https://doi.org/10.1021/cr5006167, 2015.

Lee, A. K., Zhao, R., Li, R., Liggio, J., Li, S. M., and Abbatt, J. P.: Formation of Light Absorbing Organo-Nitrogen Species from Evaporation of Droplets Containing Glyoxal and Ammonium Sulfate, Environ. Sci. Technol., 47, 12819−12826, https://doi.org/10.1021/es402687w, 2013.

Lei, Y., Lei, X., Tian, G., Yang, J., Huang, D., Yang, X., Chen, C. C., and Zhao, J. C.: Optical Variation and Molecular Transformation of Brown Carbon During Oxidation by NO_3• in the Aqueous Phase, Environ. Sci. Technol., 58, 3353−3362, https://doi.org/10.1021/acs.est.3c08726, 2024.

Li, C. L., He, Q. F., Fang, Z., Brown, S. S., Laskin, A., Cohen, S. R., and Rudich, Y.: Laboratory Insights into the Diel Cycle of Optical and Chemical Transformations of Biomass Burning Brown Carbon Aerosols, Environ. Sci. Technol., 54, 11827−11837, https://dx.doi.org/10.1021/acs.est.0c04310, 2020.

Li, F. H., Zhou, S. Z., Du, L., Zhao, J., Hang, J., and Wang, X. M.: Aqueous-phase chemistry of atmospheric phenolic compounds: A critical review of laboratory studies, Sci. Total Environ., 856, 158895, https://doi.org/10.1016/j.scitotenv.2022.158895, 2023.

Li, G., Bei, N., Tie, X., and Molina, L. T.: Aerosol effects on the photochemistry in Mexico City during MCMA-2006/MILAGRO campaign, Atmos. Chem. Phys., 11, 5169−5182, https://doi.org/10.5194/acp-11-5169-2011, 2011.

Li, Z. J., Tan, H. B., Zheng, J., Liu, L., Qin, Y. M., Wang, N., Li, F., Li ,Y. J., Cai, M. F., Ma, Y., and Chan, C. K.: Light absorption properties and potential sources of particulate brown carbon in the Pearl River Delta region of China, Atmos. Chem. Phys., 19, 11669−11685, https://doi.org/10.5194/acp-19-11669-2019, 2019.

Lim, Y. B., Tan, Y., Perri, M. J., Seitzinger, S. P., and Turpin, B. J.: Aqueous chemistry and its role in secondary organic aerosol (SOA) formation, Atmos. Chem. Phys., 10, 10521−10539, https://doi.org/10.5194/acp-10-10521-2010, 2010.

Liu, M. X., Song, Y., Zhou, T., Xu, Z. Y., Yan, C. Q., Zheng, M., Wu, Z. J., Hu, M., Wu, Y. S., and Zhu, T.: Fine particle pH during severe haze episodes in northern China, Geophys. Res. Lett., 44, 5213−5221, https://doi.org/10.1002/2017gl073210,

2017.

Liu, Y., Huang, R. J., Lin, C. S., Yuan, W., Li, Y. J., Zhong, H. B., Yang, L., Wang, T., Huang, W., Xu, W., Huang, D. D., and Huang, C.: Nitrate-Photolysis Shortens the Lifetimes of Brown Carbon Tracers from Biomass Burning, Environ. Sci. Technol., 59, 640−649, https://doi.org/10.1021/acs.est.4c06123, 2024.

Lorenzo, R. A. D., Washenfelder, R. A., Attwood, A. R., Guo, H., Xu, L., Ng, N. L., Weber, R. J., Baumann, K., Edgerton, E., and Young, C. J.: Molecular-Size-Separated Brown Carbon Absorption for Biomass-Burning Aerosol at Multiple Field Sites, Environ. Sci. Technol., 51, 3128−3137, https://doi.org/10.1021/acs.est.6b06160, 2017.

Lu, Z., Streets, D. G., Winijkul, E., Yan, F., Chen, Y., Bond, T. C., Feng, Y., Dubey, M. K., Liu, S., Pinto, J. P., and Carmichael, G. R.: Light absorption properties and radiative effects of primary organic aerosol emissions, Environ. Sci. Technol., 49, 4868−4877, https://doi.org/10.1021/acs.est.5b00211, 2015.

Luo, J. Q., Zhang, J. K., Huang, X. J ., Liu, Q., Luo, B., Zhang, W., Rao, Z. H., and Yu, Y. C.: Characteristics, evolution, and regional differences of biomass burning particles in the Sichuan Basin, China, J. Environ. Sci., 89, 35−46, https://doi.org/10.1016/j.jes.2019.09.015, 2020.

Matthew, B. M., Middlebrook, A. M., and Onasch, T. B.: Collection Efficiencies in an Aerodyne Aerosol Mass Spectrometer as a Function of Particle Phase for Laboratory Generated Aerosols, Aerosol Sci. Technol., 42, 884−898, https://doi.org/10.1080/02786820802356797, 2008.

McNeill, V. F.: Aqueous Organic Chemistry in the Atmosphere: Sources and Chemical Processing of Organic Aerosols, Environ. Sci. Technol., 49, 1237−1244, https://doi.org/10.1021/es5043707, 2015.

Meng, J. J., Liu, X. D., Hou, Z. F., Yi, Y. A., Yan, L., Li, Z., Cao, J. J., Li, J. J., and Wang, G. H.: Molecular characteristics and stable carbon isotope compositions of dicarboxylic acids and related compounds in the urban atmosphere of the North China Plain: Implications for aqueous phase formation of SOA during the haze periods, Sci. Total Environ., 705, 135256,

https://doi.org/10.1016/j.scitotenv.2019.135256, 2020.

Middlebrook, A. M., Bahreini, R., Jimenez, J. L., and Canagaratna, M. R.: Evaluation of Composition-Dependent Collection Efficiencies for the Aerodyne Aerosol Mass Spectrometer using Field Data, Aerosol Sci. Technol., 46, 258−271, https://doi.org/10.1080/02786826.2011.620041, 2012.

Ministry of Environmental Protection (MEP): P.R. Of China, China National Ambient Air Quality Standard (GB 3095-2012), http://kjs.mep.gov.cn/hjbhbz/bzwb/dqhjbh/dqhjzlbz/201203/t20120302_224165.htm, 2012.

Moosmüller, H., Chakrabarty, R. K., and Arnott, W. P.: Aerosol light absorption and its measurement: A review, J. Quant. Spectrosc. Ra., 110, 844−878, https://doi.org/10.1016/j.jqsrt.2009.02.035, 2009.

Ng, N. L., Canagaratna, M. R., Jimenez, J. L., Chhabra, P. S., Seinfeld, J. H., and Worsnop, D. R.: Changes in organic aerosol composition with aging inferred from aerosol mass spectra, Atmos. Chem. Phys., 11, 6465−6474, https://doi.org/10.5194/acp-11-6465-2011, 2011a.

Ng, N. L., Canagaratna, M. R., Jimenez, J. L., Zhang, Q., Ulbrich, I. M., and Worsnop, D. R.: Real-Time Methods for Estimating Organic Component Mass Concentrations from Aerosol Mass Spectrometer Data, Environ. Sci. Technol., 45, 910−916, https://doi.org/10.1021/es102951k, 2011b.

Ng, N. L., Canagaratna, M. R., Zhang, Q., Jimenez, J. L., Tian, J., Ulbrich, I. M., Kroll, J. H., Docherty, K. S., Chhabra, P. S., Bahreini, R., Murphy, S. M., Seinfeld, J. H., Hildebrandt, L., Donahue, N. M., DeCarlo, P. F., Lanz, V. A., Prévôt, A. S. H., Dinar, E., Rudich, Y., and Worsnop, D. R.: Organic aerosol components observed in Northern Hemispheric datasets from Aerosol Mass Spectrometry, Atmos. Chem. Phys., 10, 4625−4641, https://doi.org/10.5194/acp-10-4625-2010, 2010.

Ng, N. L., Herndon, S. C., Trimborn, A., Canagaratna, M. R., Croteau, P. L., Onasch, T. B., Sueper, D., Worsnop, D. R., Zhang, Q., Sun, Y. L., and Jayne J. T.: An Aerosol Chemical Speciation Monitor (ACSM) for Routine Monitoring of the Composition and Mass Concentrations of Ambient Aerosol, Aerosol Sci. Technol., 45, 780−794, https://doi.org/10.1080/02786826.2011.560211, 2011c.

Nguyen, T. K. V., Zhang, Q., Jimenez, J. L., Pike, M., and Carlton, A. G.: Liquid Water: Ubiquitous Contributor to Aerosol Mass, Environ. Sci. Technol. Lett., 3, 257−263, https://doi.org/10.1021/acs.estlett.6b00167, 2016.

Nozière, B., and Esteve, W.: Light-absorbing aldol condensation products in acidic aerosols: Spectra, kinetics, and contribution to the absorption index, Atmos. Environ., 41, 1150−1163, https://doi.org/10.1016/j.atmosenv.2006.10.001, 2007.

Nozière, B., Dziedzic, P., and Córdova, A.: Products and Kinetics of the Liquid-Phase Reaction of Glyoxal Catalyzed by Ammonium Ions (NH_4^+), J. Phys. Chem. A, 113, 231−237, https://doi.org/10.1021/jp8078293, 2009.

Ortega, A. M., Ortega, D. A., Cubison, M. J., Brune, W. H., Bon, D., Gouw de, J. A., and Jimenez, J. L.: Secondary organic aerosol formation and primary organic aerosol oxidation from biomass-burning smoke in a flow reactor during FLAME-3, Atmos. Chem. Phys., 13, 11551−11571, https://doi.org/10.5194/acp-13-11551-2013, 2013.

Ortiz-Montalvo, D. L., Lim, Y. B., Perri, M. J., Seitzinger, S. P., and Turpin, B. J.: Volatility and Yield of Glycolaldehyde SOA Formed through Aqueous Photochemistry and Droplet Evaporation, Aerosol Sci. Technol., 46, 1002−1014, https://doi.org/10.1080/02786826.2012.686676, 2012.

Paatero, P.: The Multilinear Engine: A Table-Driven, Least Squares Program for Solving Multilinear Problems, Including the n-Way Parallel Factor Analysis Model, J. Comput. Graph. Stat., 8, 854−888, https://doi.org/10.1080/10618600.1999.10474853, 1999.

Paatero, P. and Hopke, P. K.: Discarding or downweighting high-noise variables in factor analytic models, Anal. Chim. Acta., 490, 277−289, https://doi.org/10.1016/S0003-2670(02)01643-4, 2003.

Paatero, P. and Tapper, U.: Positive matrix factorization: A non-negative factor model with optimal utilization of error estimates of data values, Environmetrics, 5, 111−126, https://doi.org/10.1002/env.3170050203, 1994.

Paglione, M., Gilardoni, S., Rinaldi, M., Decesari, S., Zanca, N., Sandrini, S., Giulianelli, L., Bacco, D., Ferrari, S., Poluzzi, V., Scotto, F., Trentini, A., Poulain,

L., Herrmann, H., Wiedensohler, A., Canonaco, F., Prévôt, A. S. H., Massoli, P., Carbone, C., Facchini, M. C., and Fuzzi, S. C.: The impact of biomass burning and aqueous-phase processing on air quality: a multi-year source apportionment study in the Po Valley, Italy, Atmos. Chem. Phys., 20, 1233−1254, https://doi.org/10.5194/acp-20-1233-2020, 2020.

Pang, H. W., Zhang, Q., Lu, X. H., Li, K. N., Chen, H., Chen, J. M., Yang, X., Ma, Y. G., Ma, J. L., and Huang, C.: Nitrite-Mediated Photooxidation of Vanillin in the Atmospheric Aqueous Phase, Environ. Sci. Technol., 53, 14253−14263, https://doi.org/10.1021/acs.est.9b03649, 2019.

Peng, C., Tian, M., Chen, Y., Wang, H. B., Zhang, L. M., Shi, G. M., Liu, Y., Yang, F. M., and Zhai, C. Z.: Characteristics, Formation Mechanisms and Potential Transport Pathways of $PM_{2.5}$ at a Rural Background Site in Chongqing, Southwest China, Aerosol Air Qual. Res., 19, 1980−1992, https://doi.org/10.4209/aaqr.2019.01.0010, 2019.

Peng, C., Tian, M., Shi, G. M., Zhang, S. M., Long, X., Che, H. X., Zhong, J., You, X. Y., Bao, Z. E., Yang, F. M., Qi, X., Zhai, C. Z., and Chen, Y.: Sources and light absorption of brown carbon in urban areas of the Sichuan Basin, China: Contribution from biomass burning and secondary formation, Atmos. Res., 318, 107992, https://doi.org/10.1016/j.atmosres.2025.107992, 2025.

Powelson, M. H., Espelien, B. M., Hawkins, L. N., Galloway, M. M., and Haan, D. O. D.: Brown Carbon Formation by Aqueous-Phase Carbonyl Compound Reactions with Amines and Ammonium Sulfate, Environ. Sci. Technol., 48, 985−993, https://doi.org/10.1021/es4038325, 2014.

Qin, Y. M., Tan, H. B., Li, Y. J., Li, Z. J., Schurman, M. I., Liu, L., Wu, C., and Chan, C. K.: Chemical characteristics of brown carbon in atmospheric particles at a suburban site near Guangzhou, China, Atmos. Chem. Phys., 18, 16409−16418, https://doi.org/10.5194/acp-18-16409-2018, 2018.

Qiu, X., Duan, L., Chai, F., Wang, S., Yu, Q., and Wang, S.: Deriving High-Resolution Emission Inventory of Open Biomass Burning in China based on Satellite Observations, Environ. Sci. Technol., 50, 11779−11786,

https://doi.org/10.1021/acs.est.6b02705, 2016.

Saleh, R., Hennigan, C. J., McMeeking, G. R., Chuang, W. K., Robinson, E. S., Coe, H., Donahue, N. M., and Robinson, A. L.: Absorptivity of brown carbon in fresh and photo-chemically aged biomass-burning emissions, Atmos. Chem. Phys., 13, 7683−7693, https://doi.org/10.5194/acp-13-7683-2013, 2013.

Saleh, R., Robinson, E. S., Tkacik, D. S., Ahern, A. T., Liu, S., Aiken, A. C., Sullivan, R. C., Presto, A. A., Dubey, M. K., Yokelson, R. J., Donahue, N. M., and Robinson, A. L.: Brownness of organics in aerosols from biomass burning linked to their black carbon content, Nat. Geosci., 7, 647−650, https://doi.org/10.1038/ngeo2220, 2014.

Sareen, N., Moussa, S. G., and McNeill, V. F.: Photochemical Aging of Light-Absorbing Secondary Organic Aerosol Material, J. Phys. Chem. A, 117, 2987−2996, https://doi.org/10.1021/jp309413j, 2013.

Shrivastava, M., Cappa, C. D., Fan, J. W., Goldstein, A. H., Guenther, A. B., Jimenez, J. L., Kuang, C. A., Laskin, A., Martin, S. T., Ng, N. L., Petaja, T., Pierce, J. R., Rasch, P. J., Roldin, P., Seinfeld, J. H., Shilling, J., Smith, J. N., Thornton, J. A., Volkamer, R., Wang, J., Worsnop, D. R., Zaveri, R. A., Zelenyuk, A., and Zhang, Q.: Recent advances in understanding secondary organic aerosol: Implications for global climate forcing, Rev. Geophys., 55, 509−559, doi:10.1002/2016RG000540, 2017.

Sun, Y. L., Du, W., Fu, P. Q., Wang, Q. Q., Li, J., Ge, X. L., Zhang, Q., Zhu, C. M., Ren, L. J., Xu, W. Q., Zhao, J., Han, T. T., Worsnop, D. R., and Wang, Z. F.: Primary and secondary aerosols in Beijing in winter: sources, variations and processes, Atmos. Chem. Phys., 16, 8309−8329, https://doi.org/10.5194/acp-16-8309-2016, 2016a.

Sun, Y. L., Jiang, Q., Xu, Y. S., Ma, Y., Zhang, Y. J., Liu, X. G., Li, W. J., Wang, F., Li, J., Wang, P. C., and Li, Z. Q.: Aerosol characterization over the North China Plain: Haze life cycle and biomass burning impacts in summer, J. Geophys. Res.: Atmos., 121, 2508−2521, https://doi.org/10.1002/ 2015jd024261, 2016b.

Sun, Y. L., Zhang, Q., Anastasio, C., and Sun, J.: Insights into secondary organic

aerosol formed via aqueous-phase reactions of phenolic compounds based on high resolution mass spectrometry, Atmos. Chem. Phys., 10, 4809−4822, https://doi.org/10.5194/acp-10-4809-2010, 2010.

Tan, Y., Lim, Y. B., Altieri, K. E., Seitzinger, S. P., and Turpin, B. J.: Mechanisms leading to oligomers and SOA through aqueous photooxidation: insights from OH radical oxidation of acetic acid and methylglyoxal, Atmos. Chem. Phys., 12, 801−813, https://doi.org/10.5194/acp-12-801-2012, 2012.

Tang, H. H., Li, Z. L., Tian, M., Peng, C., Ding, Y., Chen, M. L., Wang, X., C., Chen, Y., Yang, F. M., and Zhai, C. Z.: Formation of Oxidized Organic Aerosols in Winter Haze in a Megacity of Southwest China: Implication for the Importance of Biomass Burning, J. Geophys. Res. Atmos., 130, e2025JD044028, https://doi.org/10.1029/2025JD044028, 2025.

Tao, J., Gao, J., Zhang, L., Zhang, R., Che, H., Zhang, Z., Lin, Z., Jing, J., Cao, J., and Hsu, S. C.: $PM_{2.5}$ pollution in a megacity of southwest China: source apportionment and implication, Atmos. Chem. Phys., c14, 8679−8699, https://doi.org/10.5194/acp-14-8679-2014, 2014.

Tian M., Liu Y., Yang F. M., Zhang L. M., Peng C., Chen Y., Shi G. M., Wang H. B., Luo B., Jiang C. T., Li B., Takeda N., and Koizumi K.: Increasing importance of nitrate formation for heavy aerosol pollution in two megacities in Sichuan Basin, southwest China, Environ. Pollut., 250, 898−905, https://doi.org/10.1016/j.envpol.2019.04.098, 2019.

Wang, G. H., Zhang, R. Y., Gomez, M. E., Yang, L. X., Zamora, M. L., Hu, M., Lin, Y., Peng, J. F., Guo, S., Meng, J. J., Li, J. J., Cheng, C. L., Hu T. F., Ren, Y. Q., Wang, Y. S., Gao, J., Cao, J. J., An, Z. S., Zhou, W. J., Li, G. H., Wang, J. Y., Tian, P. F., Marrero-Ortiz, W., Secrest, J., Du, Z. F., Zheng, J., Shang, D. J., Zeng, L. M., Shao, M., Wang, W. G., Huang, Y., Wang, Y., Zhu, Y. J., Li, Y. X., Hu, J. X., Pan, B., Cai, L., Cheng, Y. T., Ji, Y. M., Zhang, F., Rosenfeld, D., Liss, P. S., Duce, R. A., Kolb, C. E., and Molina, M. J.: Persistent sulfate formation from London Fog to Chinese haze, Proc. Natl. Acad. Sci. USA, 113, 13630−13635, https://doi.org/10.1073/pnas.1616540113, 2016.

Wang, H. B., Tian, M., Chen, Y., Shi, G. M., Liu, Y., Yang, F. M., Zhang, L. M., Deng, L. Q., Yu, J. Y., Peng, C., and Cao, X. Y.: Seasonal characteristics, formation mechanisms and source origins of $PM_{2.5}$ in two megacities in Sichuan Basin, China, Atmos. Chem. Phys., 18, 865−881, https://doi.org/10.5194/acp-18-865-2018, 2018.

Wang, H. B., Zhang, L. M., Huo, T. T., Wang, B., Yang, F. M., Chen, Y., Tian, M., Qiao, B. Q., and Peng, C.: Application of parallel factor analysis model to decompose excitation-emission matrix fluorescence spectra for characterizing sources of water-soluble brown carbon in $PM_{2.5}$, Atmos. Environ., 223, 117192, https://doi.org/10.1016/j.atmosenv.2019.117192, 2019a.

Wang, J. F., Ye, J. H., Zhang, Q., Zhao, J., Wu, Y. Z., Li, J. Y., Liu, D. T., Li, W. J., Zhang, Y. G., Wu, C., Xie, C. H., Qin, Y. M., Lei, Y. L., Huang, X. P., Guo, J. P., Liu, P. F., Fu, P. Q., Li, Y. J., Lee, H. C., Choi, H., Zhang, J., Liao, H., Chen, M. D., Sun, Y. L., Ge, X. L., Martin, S. T., and Jacob, D. J.: Aqueous production of secondary organic aerosol from fossil-fuel emissions in winter Beijing haze, Proc. Natl. Acad. Sci. USA, 118, e2022179118, https://doi.org/10.1073/pnas.2022179118, 2021.

Wang, Q. Y., Ye, J. H., Wang, Y. C., Zhang, T., Ran, W. K., Wu, Y. F., Tian, J., Li, L., Zhou, Y. Q., Ho, H. S. S., Dang, B., Zhang, Q., Zhang, R. J., Chen, Y., Zhu, C. S., and Cao, J. J.: Wintertime Optical Properties of Primary and Secondary Brown Carbon at a Regional Site in the North China Plain, Environ. Sci. Technol., 53, 12389−12397, https://doi.org/10.1021/acs.est.9b03406, 2019b.

Washenfelder, R. A., Attwood, A. R., Brock, C. A., Guo, H., Xu, L., Weber, R. J., Ng, N. L., Allen, H. M., Ayres, B. R., Baumann, K., Cohen, R. C., Draper, D. C., Duffey, K. C., Edgerton, E., Fry, J. L., Hu, W. W., Jimenez, J. L., Palm, B. B., Romer, P., Stone, E. A., Wooldridge, P. J., and Brown, S. S.: Biomass burning dominates brown carbon absorption in the rural southeastern United States, Geophys. Res. Lett., 42, 653−664, https://doi.org/10.1002/2014gl062444, 2015.

Wu, C. and Yu, J. Z.: Determination of primary combustion source organic carbon-to-elemental carbon (OC/EC) ratio using ambient OC and EC measurements: Secondary OC-EC correlation minimization method, Atmos. Chem.

Phys., 16, 5453−5465, https://doi.org/10.5194/acp-16-5453-2016, 2016.

Wu, H., Peng, C., Zhai, T. Y., Deng, J. C., Lu, P. L., Li, Z. L., Chen, Y., Tian, M., Bao, Z. E., Long, X., Yang, F. M., and Zhai, C. Z.: Characteristics of light absorption and environmental effects of Brown carbon aerosol in Chongqing during summer and winter based on online measurement: Implications of secondary formation, Atmos. Environ., 338, 120843, https://doi.org/10.1016/j.atmosenv.2024.120843, 2024.

Xie, C. H., Xu, W. Q., Wang, J. F., Wang, Q. Q., Liu, D. T., Tang, G. Q., Chen, P., Du, W., Zhao, J., Zhang, Y. J., Zhou, W., Han, T. T., Bian, Q. Y., Li, J., Fu, P. Q., Wang, Z. F., Ge, X. L., Allan, J., Coe, H., and Sun, Y. L.: Vertical characterization of aerosol optical properties and brown carbon in winter in urban Beijing, China, Atmos. Chem. Phys., 19, 165−179, https://doi.org/10.5194/acp-19-165-2019, 2019.

Xu, B. Q., Zhang, G., Gustafsson, Ö., Kawamura, K., Li, J., Andersson, A., Bikkina, S., Kunwar, B., Pokhrel, A., Zhong, G. C., Zhao, S. Z., Li, J., Huang, C., Cheng, Z. N., Zhu, S. Y., Peng, P. A., and Sheng, G. Y.: Large contribution of fossil-derived components to aqueous secondary organic aerosols in China, Nat. Commun., 13, 5115, https://doi.org/10.1038/s41467-022-32863-3, 2022.

Xu, W. Q., Han, T. T., Du, W., Wang, Q. Q., Chen, C., Zhao, J., Zhang, Y. J., Li, J., Fu, P. Q., Wang, Z. F., Worsnop, D. R., and Sun, Y. L.: Effects of Aqueous-Phase and Photochemical Processing on Secondary Organic Aerosol Formation and Evolution in Beijing, China, Environ. Sci. Technol., 51, 762−770, https://doi.org/10.1021/acs.est.6b04498, 2017.

Xu, W. Q., Sun, Y. L., Chen, C., Du, W., Han, T. T., Wang, Q. Q., Fu, P. Q., Wang, Z. F., Zhao, X. J., Zhou, L. B., Ji, D. S., Wang, P. C., and Worsnop, D. R.: Aerosol composition, oxidation properties, and sources in Beijing: results from the 2014 Asia-Pacific Economic Cooperation summit study, Atmos. Chem. Phys., 15, 13681−13698, https://doi.org/10.5194/acp-15-13681-2015, 2015.

Xu, W. Q., Sun, Y. L., Wang, Q. Q., Zhao, J., Wang, J. F., Ge, X. L., Xie, C. J., Zhou, W., Du, W., Li, J., Fu, P. Q., Wang, Z. F., Worsnop, D. R., and Coe, H.: Changes in Aerosol Chemistry From 2014 to 2016 in Winter in Beijing: Insights From

High-Resolution Aerosol Mass Spectrometry, J. Geophys. Res.: Atmos., 124, 1132−1147, https://doi.org/10.1029/2018JD029245, 2019.

Yan, C. Q., Zheng, M., Bosch, C., Andersson, A., Desyaterik, Y., Sullivan, A. P., Collett, J. L., Zhao, B., Wang, S. X., He, K. B., and Gustafsson, Ö.: Important fossil source contribution to brown carbon in Beijing during winter, Sci. Rep., 7, 43182, https://doi.org/10.1038/srep43182, 2017.

Yang, F. M., Tan, J., Zhao, Q., Du, Z., He, K. B., Ma, Y. L., Duan, F. K., Chen, G., and Zhao, Q.: Characteristics of $PM_{2.5}$ speciation in representative megacities and across China, Atmos. Chem. Phys., 11, 5207−5219, https://doi.org/10.5194/acp-11-5207-2011, 2011.

Yang, J. W., Au, W. C., Law, H., Lam, C. H., and Nah, T.: Formation and evolution of brown carbon during aqueous-phase nitrate-mediated photooxidation of guaiacol and 5-nitroguaiacol, Atmos. Environ., 254, 118401, https://doi.org/10.1016/j.atmosenv.2021.118401, 2021.

Yang, W., Xie, S., Zhang, Z., Hu, J., Zhang, L., Lei, X., Zhong, L., Hao, Y., and Shi, F.: Characteristics and sources of carbonaceous aerosol across urban and rural sites in a rapidly urbanized but low-level industrialized city in the Sichuan Basin, China, Environ. Sci. Pollut. R., 26, 26646−26663, https://doi.org/10.1007/s11356-019-05242-7, 2019.

Ye, Z. L., Qu, Z. X., Ma, S. S., Luo, S. P., Chen, Y. T., Chen, H., Chen, Y. F., Zhao, Z. Z., Chen, M. D., and Ge, X. L.: A comprehensive investigation of aqueous-phase photochemical oxidation of 4-ethylphenol, Sci. Total Environ., 685, 976−985, https://doi.org/10.1016/j.scitotenv.2019.06.276, 2019.

Yokelson, R. J., Urbanski, S. P., Atlas, E. L., Toohey, D. W., Alvarado, E. C., Crounse, J. D., Wennberg, P. O., Fisher, M. E., Wold, C. E., Campos, T. L., Adachi, K., Buseck, P. R., and Hao, W. M.: Emissions from forest fires near Mexico City, Atmos. Chem. Phys., 7, 5569−5584, https://doi.org/10.5194/acp-7-5569-2007, 2007.

Yu, L., Smith, J., Laskin, A., Anastasio, C., Laskin, J., Zhang, Q.: Chemical characterization of SOA formed from aqueous-phase reactions of phenols with the

triplet excited state of carbonyl and hydroxyl radical, Atmos. Chem. Phys., 14, 13801−13816, https://doi.org/10.5194/acp-14-13801-2014, 2014.

Yu, L., Smith, J., Laskin, A., George, K. M., Anastasio, C., Laskin, J., Dillner, A. M., and Zhang, Q.: Molecular transformations of phenolic SOA during photochemical aging in the aqueous phase: competition among oligomerization, functionalization, and fragmentation, Atmos. Chem. Phys., 16, 4511−4527, https://doi.org/10.5194/acp-16-4511-2016, 2016.

Zeng, X., Bao, Z., Zhou, J., Shi, G., Zhou, L., Zhang, S., Qi, X., Lu, K., Zhai, C., Li, Z., Li, X., Peng, C., Yang, F., Tang, M., Feng, M., Tan, Q., and Chen, Y.: Effects of photochemical and aqueous-phase oxidation on secondary formation during the 31st FISU Summer World University Games, 2023, J. Environ. Sci., 162, 810−820, https://doi.org/10.1016/j.jes.2025.08.039, 2025.

Zhang, X. Y., Bao, Z. R., Zhang, L. Y., Zhou, J. W., Che, H. X., Li, Q., Tian, M., Yang, F. M., and Chen, Y.: Biomass burning and aqueous reactions drive the elevation of wintertime $PM_{2.5}$ in the rural area of the Sichuan basin, China, Atmos. Environ., 306, 119779, https://doi.org/10.1016/j.atmosenv.2023.119779, 2023.

Zhang, X. Y., Liu, H. X., Cheng, J. L., Song, W., Wang, H. C., Zhang, Y. L., and Wang, X. M.: Gas-Phase Oxidation of Guaiacol by NO_3 Radicals: Kinetic Measurements and Implications, ACS ES&T Air, 2, 903−910, https://doi.org/10.1021/acsestair.4c00353, 2025.

Zhao, J., Du, W., Zhang, Y. J., Wang, Q. Q., Chen, C., Xu, W. Q., Han, T. T., Wang, Y. Y., Fu, P. Q., Wang, Z. F., Li, Z. Q., and Sun, Y. L.: Insights into aerosol chemistry during the 2015 China Victory Day parade: results from simultaneous measurements at ground level and 260 m in Beijing, Atmos. Chem. Phys., 17, 3215−3232, https://doi.org/10.5194/acp-17-3215-2017, 2017.

Zhao, J., Qiu, Y. M.,Zhou, W., Xu, W. Q., Wang, J. F., Zhang, Y. J., Li, L. J., Xie, C. H., Wang, Q. Q., Du, W., Worsnop, D. R., Canagaratna, M. R., Zhou, L. B., Ge, X. L., Fu, P. Q., Li, J., Wang, Z. F., Donahue, N. M., and Sun, Y. L.: Organic Aerosol Processing During Winter Severe Haze Episodes in Beijing, J. Geophys. Res.: Atmos., 124, 10248−10263, https://doi.org/10.1029/2019JD030832, 2019.

Zhao, R., Lee, A. K. Y., Huang, L., Li, X., Yang, F., and Abbatt, J. P. D.: Photochemical processing of aqueous atmospheric brown carbon, Atmos. Chem. Phys., 15, 6087−6100, https://doi.org/10.5194/acp-15-6087-2015, 2015.

Zhao, R., Mungall, E. L., Lee, A. K. Y., Aljawhary, D., and Abbatt, J. P. D.: Aqueous-phase photooxidation of levoglucosan – a mechanistic study using aerosol time-of-flight chemical ionization mass spectrometry (Aerosol ToF-CIMS), Atmos. Chem. Phys., 14, 9695−9706, https://doi.org/10.5194/acp-14-9695-2014, 2014.

Zhong, H. B., Huang, R. J., Chang, Y. H., Duan, J., Lin, C. S., and Chen, Y.: Enhanced formation of secondary organic aerosol from photochemical oxidation during the COVID-19 lockdown in a background site in Northwest China, Sci. Total Environ., 778, 144947, https://doi.org/10.1016/j.scitotenv.2021.144947, 2021.

Zhu, C. S., Cao, J. J., Hu, T. F., Shen, Z. X., Tie, X. X., Huang, H., Wang, Q. Y., Huang, R. J., Zhao, Z. Z., Mocnik, G., and Hansen, A. D. A.: Spectral dependence of aerosol light absorption at an urban and a remote site over the Tibetan Plateau, Sci. Total Environ., 590−591, 14−21, https://doi.org/10.1016/j.scitotenv.2017.03.057, 2017.

Zhu, L. W., Cui, Y. J., Ge, X. L., Ye, Z. l., and Zhao, Z. Z.: Aqueous-phase photochemical oxidation of extracted WSOC in $PM_{2.5}$ from biomass burning, China Environ. Sci., 43, 1014−1025, https://doi.org/10.19674/j.cnki.issn1000-6923.20220928.004, 2023.